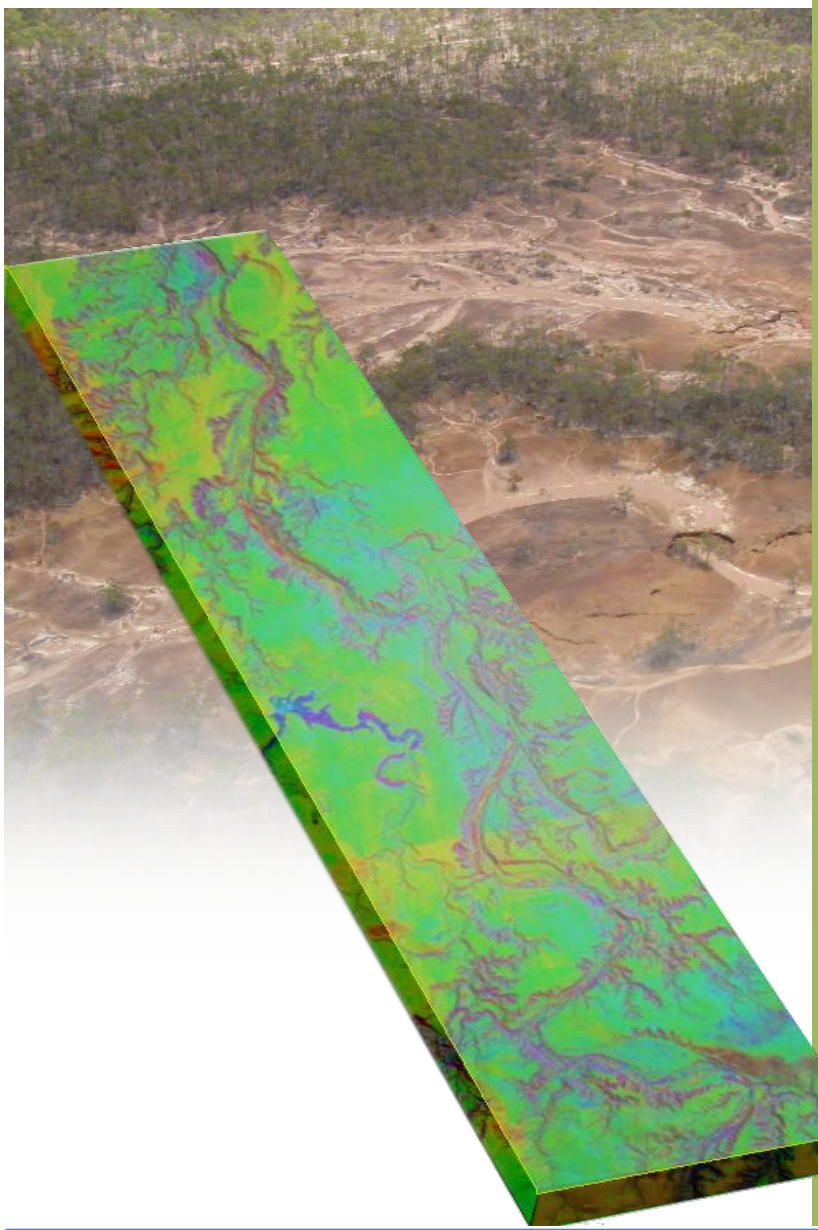

An Empirically-based Sediment Budget for the Normanby Basin

Andrew Brooks, John Spencer, Jon Olley, Tim Pietsch, Daniel Borombovits, Graeme Curwen, Jeff Shellberg, Christina Howley, Angela Gleeson, Andrew Simon, Natasha Bankhead, Danny Klimetz, Leila Eslami-Endargoli, Anne Bourgeault

Australian Rivers Institute

Griffith University

Appendix 03: LiDAR Data, Gully Mapping & LiDAR Change Detection for Determination of Sub-Surface Sediment Sources

Griffith UNIVERSITY

CARING FOR OUR COUNTRY

Appendix to the Final Report prepared for the Australian Government's Caring for our Country - **Reef Rescue initiative**

IMPORTANT

This document is current at the date noted. Due to the nature of collaborative academic publishing, this content is subject to change and revision. Please see the Cape York Water Quality website for more info:
http://www.capeyorkwaterquality.info

This Version: 3/03/2013

CAPE YORK WATER QUALITY

Appendix 03: LiDAR Data, Gully Mapping & LiDAR Change Detection for Determination of Sub-Surface Sediment Sources

Prepared by: Graeme Curwen, Andrew Brooks, John Spencer, Anne Bourgeault, Leila Eslami Endargoli & David Moore

1. LiDAR Data Acquisition

A total of 50 blocks of LiDAR were flown between May and August 2009 by Terranean (now RPS); covering a total area of 1065.4 km2. This includes 45 blocks in the Normanby (782.5 km2), 5 blocks in the Stewart (88.9 km2), 3 blocks in the Jeannie (107.1 km2) and 1 block in the Annan (86.7 km2) (figure 1).

The Normanby catchment has an area of 24,353 km2; the 2009 LiDAR covered 3.2% of the catchment. A subset of the LiDAR blocks was re-flown the on 16th and 17th September 2011. The areas with both 2009 and 2011 LiDAR data comprised 14 blocks covering 163.1 km2, which is 0.7% of the catchment.

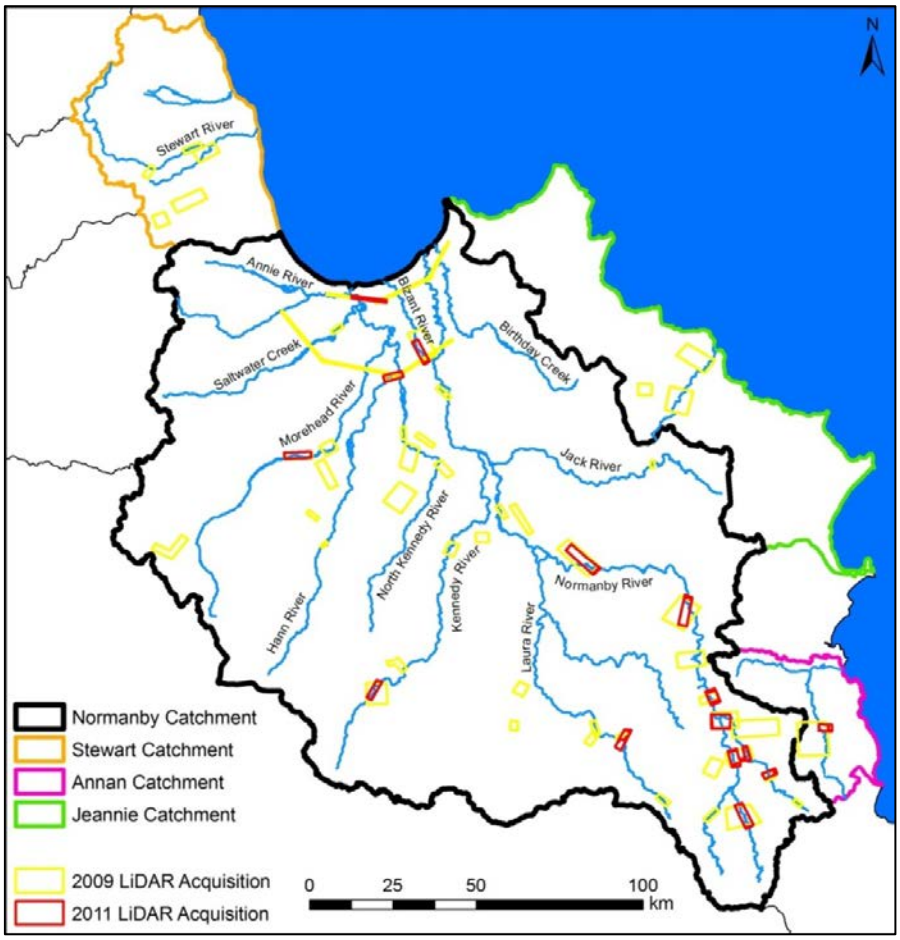

Figure 1: LiDAR blocks in the Normanby and adjacent catchments.

1.1 Flight Planning and Aerial Survey

A flight plan was developed in Takker flight management software. The flight plan consists of flight lines designed to achieve the required point density of 2.3 points per square metre and 43% overlap over the project areas. The flying height was (nominally) 600 metres above ground level.

Aerial operations were planned to give priority to collecting LiDAR within the scheduled timeframe, photography was a lesser priority to avoid delays and cost over runs in this remote area. As a result the survey was not delayed due to cloud and or restricted to times of the day when the sun is high and shadows short. Therefore the quality of the photography is not always optimal. The images were however of sufficient quality to assist interpretation and assessment of dead timber in river channels etc.

Table 1: LiDAR acquisition specifications for the 2009 data acquisition.

Sensor System 2009 data	LiDAR H56		
Parameter	Value	Unit	Comment
Viewing Angle	60	degrees	Ok
	1.05	rad	Calculated
Flight Speed	55	m/s	Ok
	198	km/h	Calculated
	107	kts	Calculated
Flight Height	660	m	Ok
Scan Rate	80	Hz	Ok
Pulse Rate	160	kHz	Ok
	860	m	Maximum Flight Altitude @ Pulse Rate
Calculated Swath Width	762	m	Calculated (434m net)
LiDAR Overlap	43	%	OK
Calculated Productivity	151	sqkm/hour	Calculated without turns
Calculated Point Spacing	0.69	m (along track)	Calculated
Calculated Point Spacing	0.57	m (across track)	Calculated
Calculated Point Density	2.54	per sqm	Calculated
Cumulative Point Density	4.73	total per sqm	Calculated
Calculated Spot Footprint	0.33	m	Calculated

Table 2: LiDAR acquisition specifications for the 2011 data acquisition.

Sensor System 2011 data	H68i	
Parameter	Value	Unit
Viewing Angle	60	degrees
	1.05	rad
Flight Speed	70	m/s
	252	km/h
	136	kts
Flight Height	850	m
Scan Rate	96	Hz
Pulse Rate	240	kHz
Calculated Swath Width	981	m
LiDAR Overlap	50	%
Calculated Productivity	247	sqkm/hour
Calculated Point Spacing	0.73	m (along track)
Calculated Point Spacing	0.59	m (across track)
Calculated Point Density	2.33	per sqm
Cumulative Point Density	4.66	total per sqm
Calculated Spot Footprint	0.43	m

Table 3: Digital Photography specifications for the 2009 & 2011 data acquisition.

Camera		
Parameter	Value	Unit
Max. Exp. Rate	3	sec
Pixel Coverage	0.085	m
Number of Frames	6.6	per km^2
Total # of Images	4760	
Min. End Lap	30	%
Min. Side Lap	25	%
Actual Side Lap	30	%
Configuration Error	OK	

1.2 Data Processing

The LiDAR waveform signal was formed into a point cloud and adjusted using the processed airborne GPS data. These adjustments are also applied to the images when establishing the image orientations prior to ortho-rectification.

Initially, the 2009 and 2011 LiDAR were adjusted separately, but it was found that horizontal and vertical displacements between the 2009 and 2011 data (i.e. error) obscured the actual surface changes in the terrain surface (i.e. the erosion signal that was the primary objective of the analysis). Consequently the 2011 data were reprocessed so that each strip was adjusted horizontally and vertically to the 2009 data. This created a better match

between the datasets, but there were very few vertical features such as buildings that could be used to reference the two datasets together.

The LiDAR points were classified as ground and non-ground points using automatic filtering followed by interactive checking and re-classification. The automatic classification applied in 2009 used TopPit software, whilst in 2011 the automatic classification was performed using TerraScan software. The differences in method used by these software packages resulted in differences in the classification of ground points and hence the terrain surfaces were not directly comparable, particularly on the edges of gullies. Therefore the 2009 data were reclassified in TerraScan to produce more closely matching terrain surfaces.

Once the point clouds had been formed and classified. Raster surfaces with 1 x 1 metre cell size were generated from the LiDAR LAS files. The rasters were provided in ESRI ASCI grid format. The following raster surfaces were produced from both the 2009 and 2011 data.

- DEM Digital Elevation Surface (Terrain Surface).
- CHM Canopy Height Model (maximum height of vegetation above the ground).
- PLR Percentage LiDAR Returns (the number of non-ground LiDAR points) returned from each pixel as a percentage of the LiDAR pulses falling on that pixel.

In addition, changes in the terrain were calculated as a surface representing the difference between the 2009 and 2011 DEMs. This data was provided as a one metre grid in ESRI ASCI Grid format and a relief shaded colour enhancement that was used for assessing the data for internal QA and was provided in ESRI compatible JP2000 format.

The photographic images were ortho rectified against the LiDAR DEM using orientations calculated from the Applanix airborne position and attitude system. The images were colour balanced and mosaicked using OrthoMaster software. The digital otho-photo mosaics have a ground pixel spacing of 12.5cm. The following steps are applied in the data processing:

1.2.1 Pre-Processing

1. Apply GPS and IMU corrections to the LiDAR data using TerraPOS adjustments and base station GPS.
2. Form points cloud from the full waveform LiDAR signal. A number of parameters can be adjusted to increase the sensitivity of the LiDAR classification to foliage and increase vertical resolution.
3. Adjust 2011point cloud to match 2009 point cloud.
4. Calculate exterior orientations for images from adjusted GPS and IMU.

1.2.2 DSM for Ortho-Rectification

1. Filter “first echo” points (eg.) 3 metres above neighbours to remove spurious points due to insects and birds etc.
2. Generate Digital Surface Model from filtered last echoes for ortho-rectification.

1.2.3 Image Ortho-Rectification and Mosaicing

1. Ortho rectify images. Horizontal adjustments determined from LiDAR are applied to the images.
2. QA to check misalignment on seams and colour mismatch.
3. QA to check horizontal displacements against ground check points.
4. Export images to required format.
5. Create metadata.
6. Final QA.

1.2.4 DEM

1. Automatic ground classification to LiDAR in TerraScan Software.
2. Perform manual editing to improve classification of ground and non-ground points.
3. Generate DEM by triangulation.
4. QA and interactive reclassification of points by reference to relief shading.
5. Export DEMs to required format (ASCII grid).
6. Final QA.

1.2.5 CHM (Canopy Height Model)

1. Filter first echoes within 10cm of DEM to produce non-ground first echo points. Last echoes have already been filtered to remove airborne objects (eg birds) and artefacts.
2. Interpolate Canopy Elevation Model (CEM) from filtered first echo points.
3. Subtract DEM from Canopy Elevation Model to produce Canopy Height Model.
4. Export CHM to required format (ASCII grid).
5. Final QA.

1.2.6 Foliage Projected Cover

1. Generate raster surfaces representing the percentage of non-ground points per square meter.
2. Export FPC rasters to required formats (ASCII grid).
3. Create metadata.
4. Final QA.

2. Gully Mapping

2.1 Google Earth Mapping

Previous attempts to map alluvial gullies through remote sensing in a similar landscape have met with mixed success (Brooks et al., 2007; Brooks et al., 2008) and in this instance it was decided that manually digitising bare ground gullies in Google Earth was a more efficient, accurate and cost effective method for determining the broad distribution of gullies across the catchment. The majority of the catchment in Google Earth is now covered by 2.5m resolution SPOT imagery, with a significant proportion of the catchment now covered by ~1m resolution Quickbird imagery. These resolutions are sufficient to map bare earth gullies that have a width of ~5m and greater. Figure 2 shows an example of hand

digitised gullies on the Google Earth imagery. The area shown contains a boundary between the two sources of satellite imagery, i.e. 2.5m SPOT and ~1m Quickbird. Digitizing across imagery with different resolutions requires a significant effort to maintain a consistent dataset across the whole catchment.

Figure 2: Example of gully digitizing on Google Earth imagery. Note the boundary between the two sources of satellite imagery, i.e. the 2.5m SPOT and the ~1m Quickbird, through the middle of the image.

A total of 9670 gullies were digitised, minimum area 3m^2, maximum area 12.7 ha, mean area 0.16 ha and total area 1566.7 ha, which is 0.06% of the Normanby catchment. Figure 4shows the gully mapping derived from Google Earth imagery produced for this project.

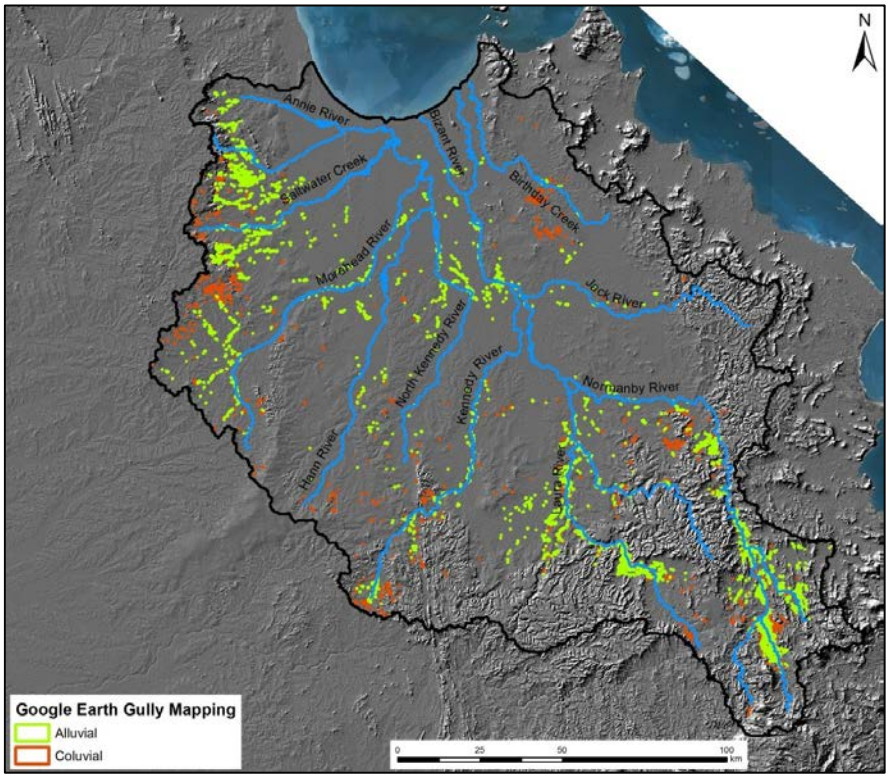

Figure 3: Distribution of gullies mapped from Google Earth in the Normanby catchment.

A comparison of Google Earth mapped gullies and LiDAR mapped gullies (described below) showed that the Google Earth mapping underestimates the extent of gullies, on average, by a factor of 7.6 (table 4, figure 5). The difference is due to the amount of gully that is covered by vegetation, which cannot be seen in satellite imagery, but is captured in LiDAR data. Therefore we consider the Google Earth gully mapping as a minimum gully extent.

Table 4: Repeat LiDAR blocks showing the extent of mapped alluvial gully from LiDAR data and Google Earth (GE).

LiDAR Block #	LiDAR gully area (ha)	GE gully area (ha)	Ratio of LiDAR gully area to GE gully area
N2	117.57	0.04	2654.4
N4	223.20	27.98	8.0
N5	344.79	39.57	8.7
N7	229.07	70.65	3.2
N9	76.96	5.86	13.1
N10	122.81	7.26	16.9
N13	246.38	22.64	10.9
N14	126.99	24.81	5.1
N16	158.06	30.35	5.2
N17	37.43	1.76	21.2
N20	147.50	12.16	12.1
N21	29.12	1.07	27.3
N25	8.52	0.11	76.5
N40	0.58	0.45	1.3
total	**1868.98**	**244.71**	**7.6**

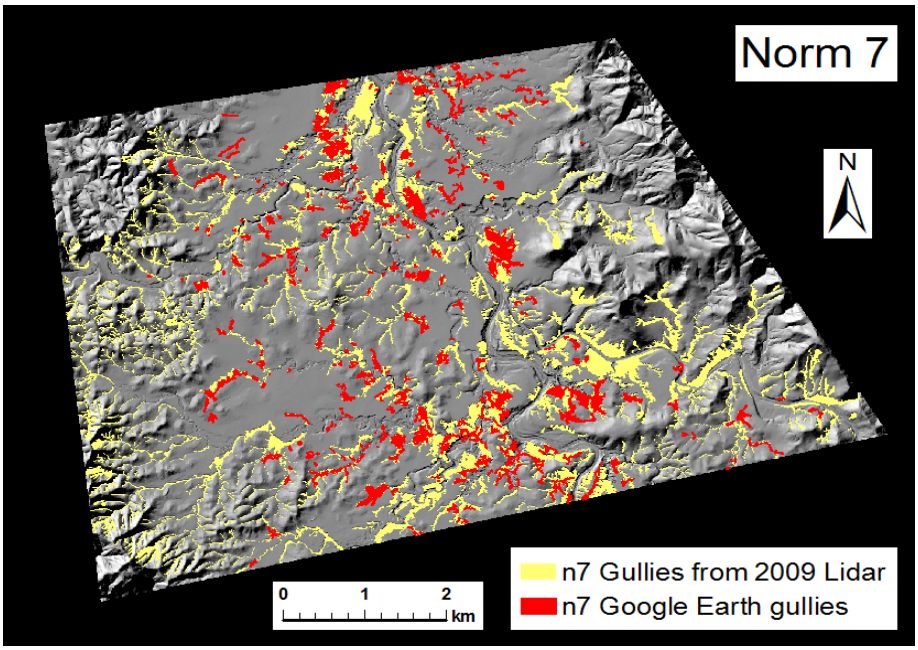

Figure 4: Hillshade relief image of LiDAR block 7. Shown here is the extent of gullies as mapped on Google Earth imagery and as mapped on LiDAR DEM data.

2.2 LiDAR Gully Mapping

A total of 16,959 features were hand digitised on hillshade relief rasters generated from the 2009 LiDAR data, defining features in the landscape formed by fluvial processes; including water bodies, bars on open riverbed, vegetated bars, benches, terraces, floodplains, gullies, banks, islands, secondary channels. The use of image segmentation software to delineate these features was attempted but it was found this was too complex a task for such an automated process and that hand digitizing gave a better delineation of features. The area of fluvial features digitised from 2009 LiDAR was 126.84km^2 which is 0.5% of the Normanby catchment. Figure 5 shows an example of digitized features.

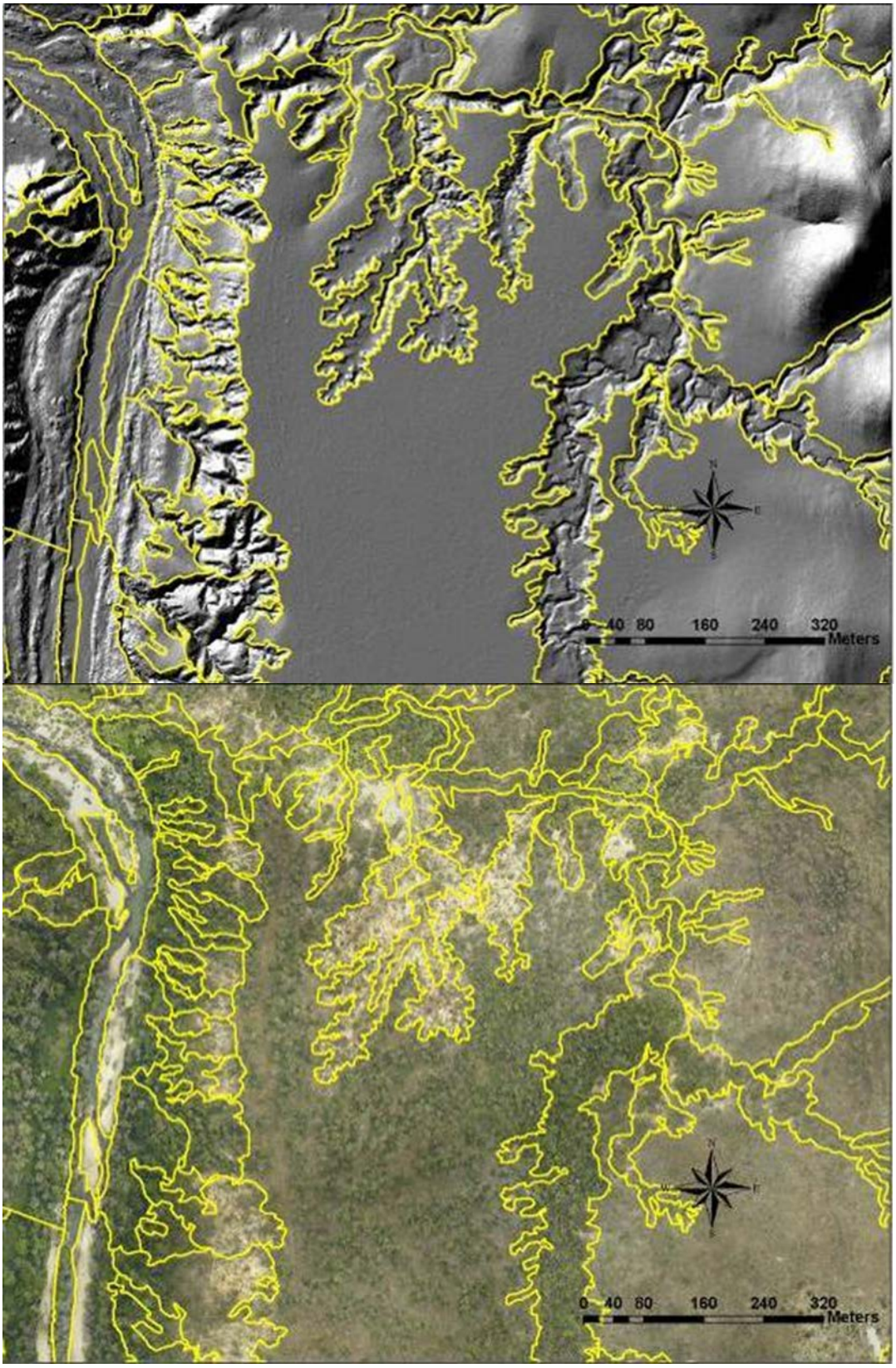

Figure 5: Example of digitising of features on a hillshade relief image (top). The same area is shown (bottom) with the ortho-photo mosaic (capture simultaneously during LiDAR acquisition) displayed. This location is on the upper-mid reaches of the Normanby. Within the alluvial gully in the centre of the image can be seen a gully inset within a gully, this is an example of the multiple phases of gully activity which are evident in parts of the catchment.

3. Landscape Units

3.1 Landscape Unit Classification within LiDAR Blocks

To differentiate between erosion processes, the effects of which were measured in the change detection analysis undertaken between the 2009 and 2011 LiDAR data (described below), the features digitised in each block were classified into functional landscape units (geomorphic units – sensu Brierley & Fryirs, (2005)). Table 5 describes the geomorphic units used in this classification and figure 6 through to figure 15 show examples of the classification of these units within Normanby LiDAR block 7.

Table 5: Descriptions of the classification system for Normanby LiDAR blocks.

Classification	Classification Code	Description
Water Bodies	1	Water present as seen in ortho-photo or discernible in hillshade relief raster.
Open River Bed	2	Main channel bed of predominantly sand, stones or rock. Sparse vegetation may be present.
Main Channel Banks	3	Obvious changes in land height between different levels within the main channel system.
Vegetated Channel Bed	4	Adjacent to main channel, covered with low or tall vegetation, fluvial scour visible in hillshade relief images, likely to be covered by average flood flows.
Gullies	5	Discrete erosional "channels" cutting into banks, floodplain or hillside. They have a clearly defined head scarp and are cutting into uneroded land surfaces.
Secondary Alluvial Channels	6	These are small tributary channels flowing through alluvium which may or may not have directly connected feeder gullies. They differ from gullies in that they clearly have a defined channel that exhibits various fluvial landforms typically associated with self-formed alluvial channels – namely floodplains, meanders, cutoffs, chutes, and in-channel bars. They may also have distinct riparian vegetation.
Road Reserve	7	Roads, road drains and areas associated with roads.
Main channel Inset Floodplain	8	Flat or nearly flat vegetated surfaces that are adjacent to the main channel. These surfaces are above the main channel, but below the high bank. The surface at the level of the high bank is almost never inundated.
Secondary Channel Inset Floodplain	9	This is the distinct floodplain associated with the secondary channels described in (6) above. The features in (6) are a composite of the channel and floodplain, whereas in some instances the floodplain and channel were mapped and classified separately. Never the less, any erosion occurring within either class 6 or 9 is ultimately lumped together as secondary channel erosion.

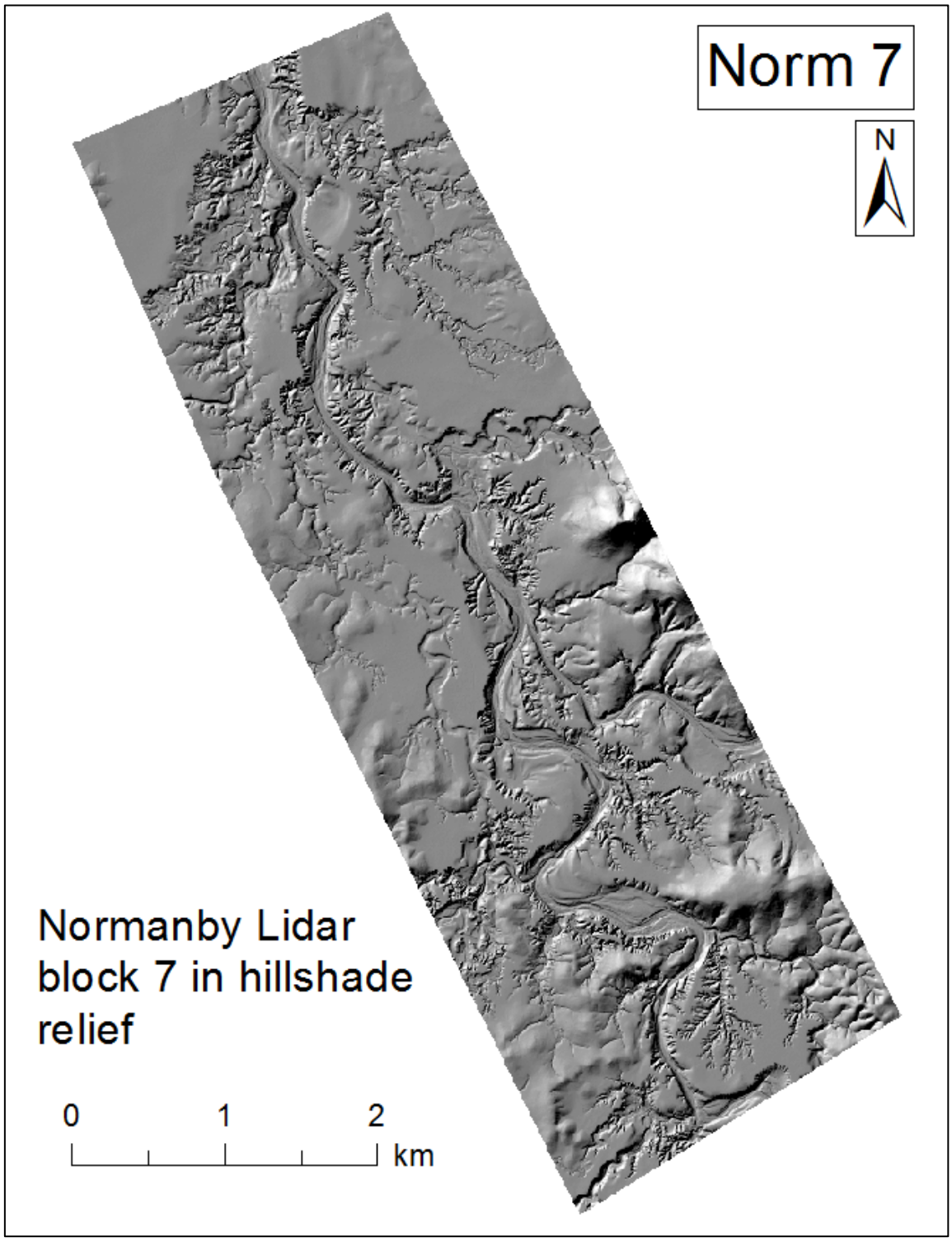

Figure 6: Normanby LiDAR block 7. This image shows the complex landscape that evolves through the different stages of development of the dendritic gully and channel networks.

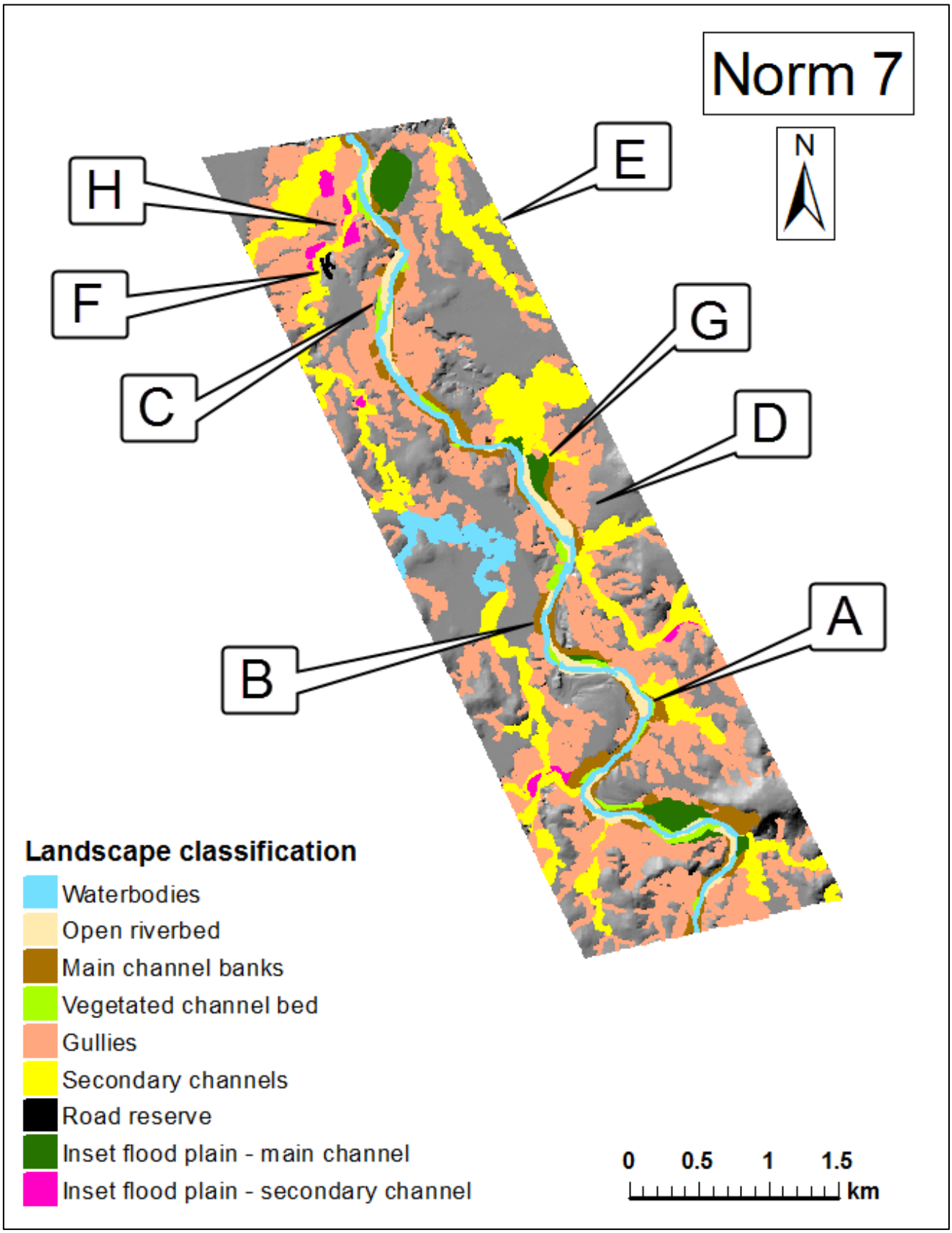

Figure 7: Normanby LiDAR block 7 overlain with landscape classification. The locations labelled A to H are referred to in figure 8 to figure 15.

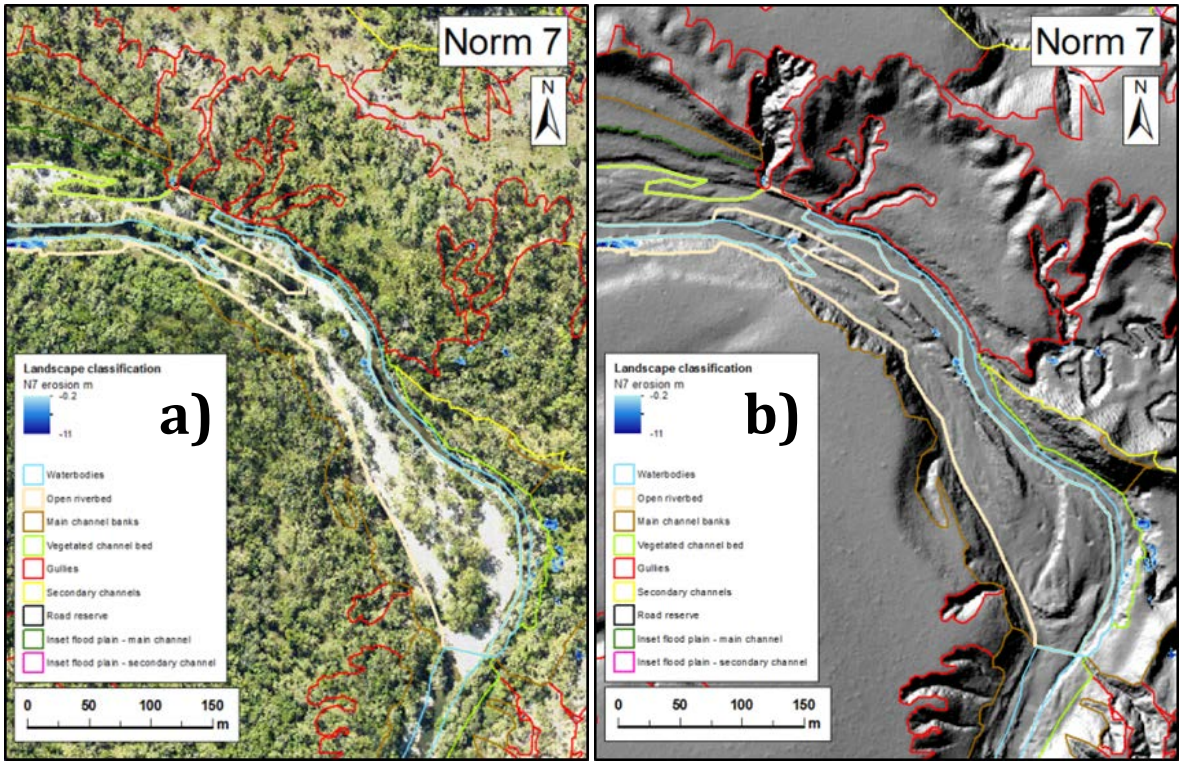

Figure 8: Location A (figure 7). Class 2 – Open River Bed in a) orthophoto and b) hillshade. Accumulation of highly reflective gravels and sand on inside (lower left of picture) and outside (upper right) of bend, 100m wide at widest; sparse vegetation grows on elevated berms and bars within the open river bed.

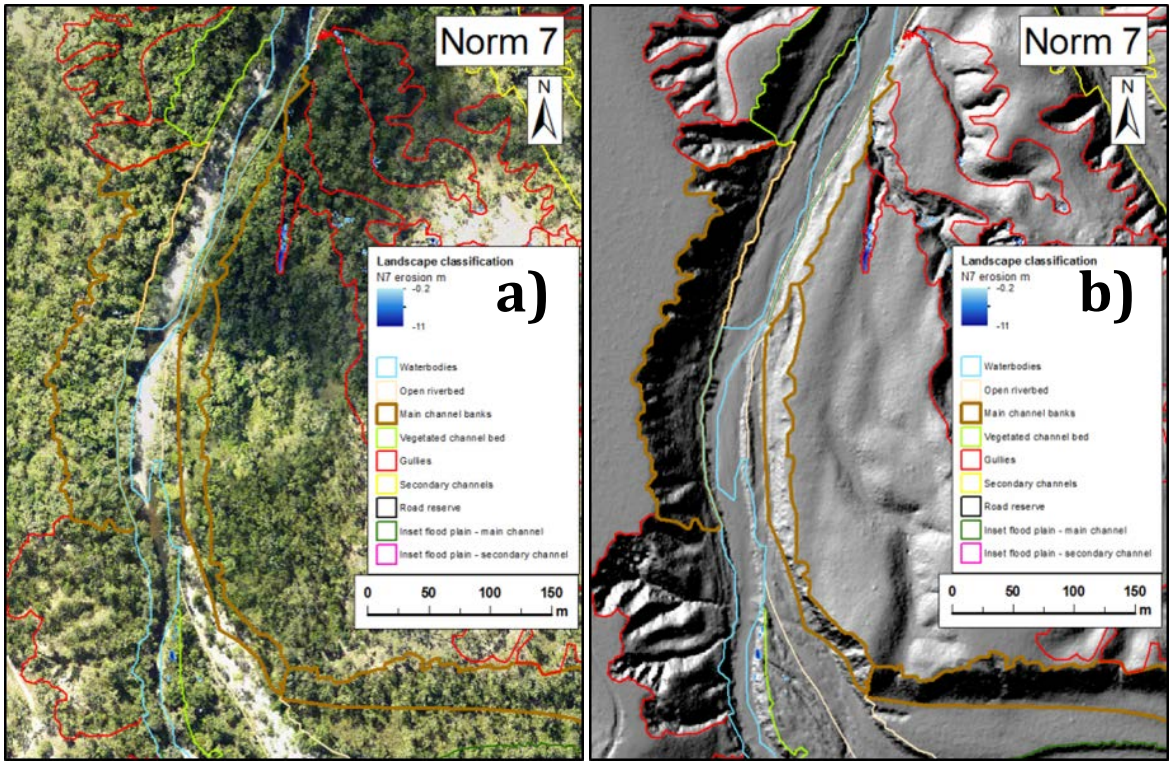

Figure 9: Location B (figure 7). Class 3 – Main Channel Banks. Transition zone from one relatively flat surface to another relatively flat surface with minimal disturbance from advanced gully erosion. Change of height may vary from low (1m height difference from water level to inset floodplain) to high (22m height difference from water level to upper floodplain surface). Usually vegetated.

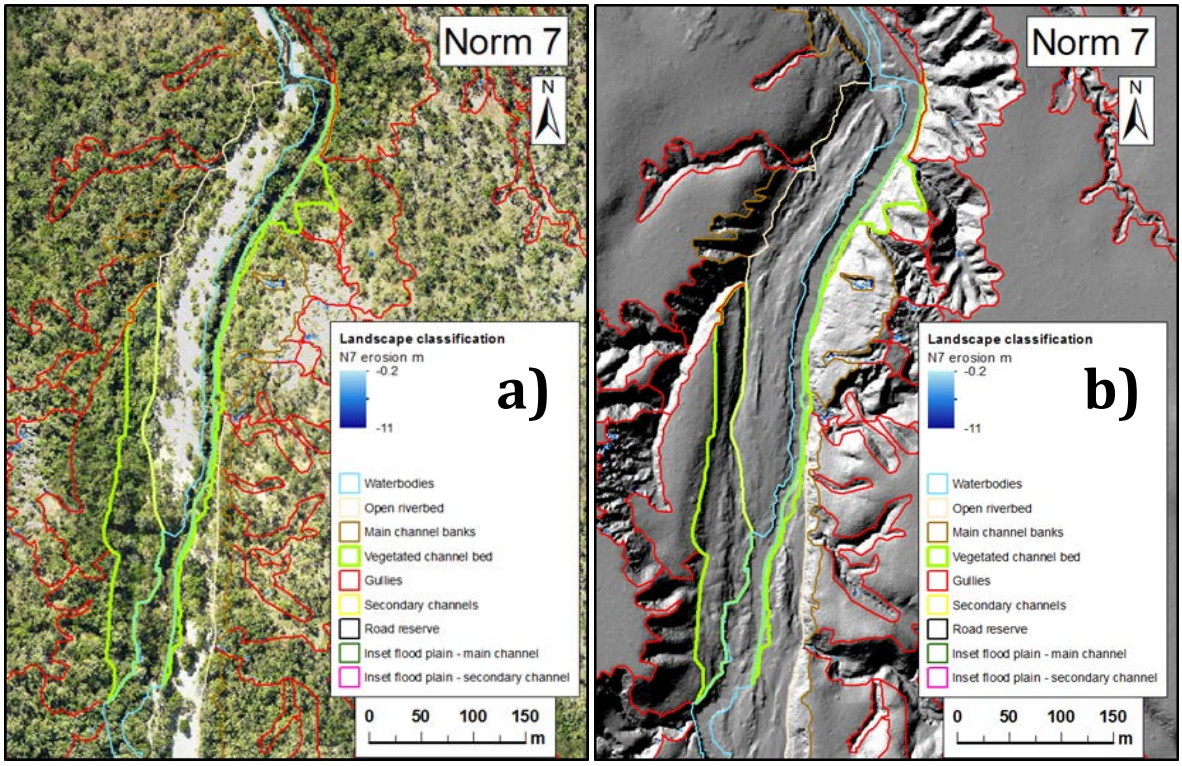

Figure 10: Location C (figure 7). Class 4 – Vegetated Channel Bed. May be continuous narrow strips of vegetation along edges of water bodies, or wider areas of riverbed with dense riparian vegetation. Fluvial scour of the channel bed is visible in b).

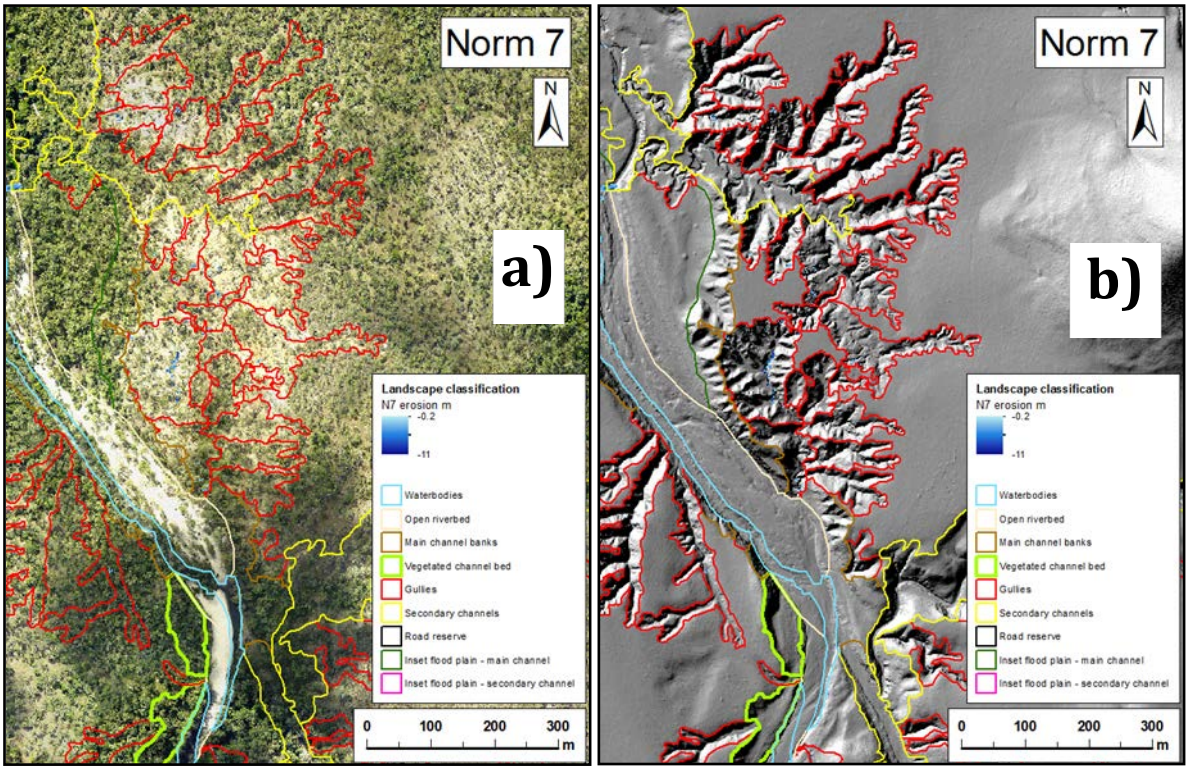

Figure 11: Location D (figure 7). Class 5 – Gullies. Gullies at different stages of development can be clearly seen in b), but are not so clearly visible in a) where vegetation obscures the gully perimeter. Out flow from several gullies may develop into flat bottomed channels with high sinuosity.

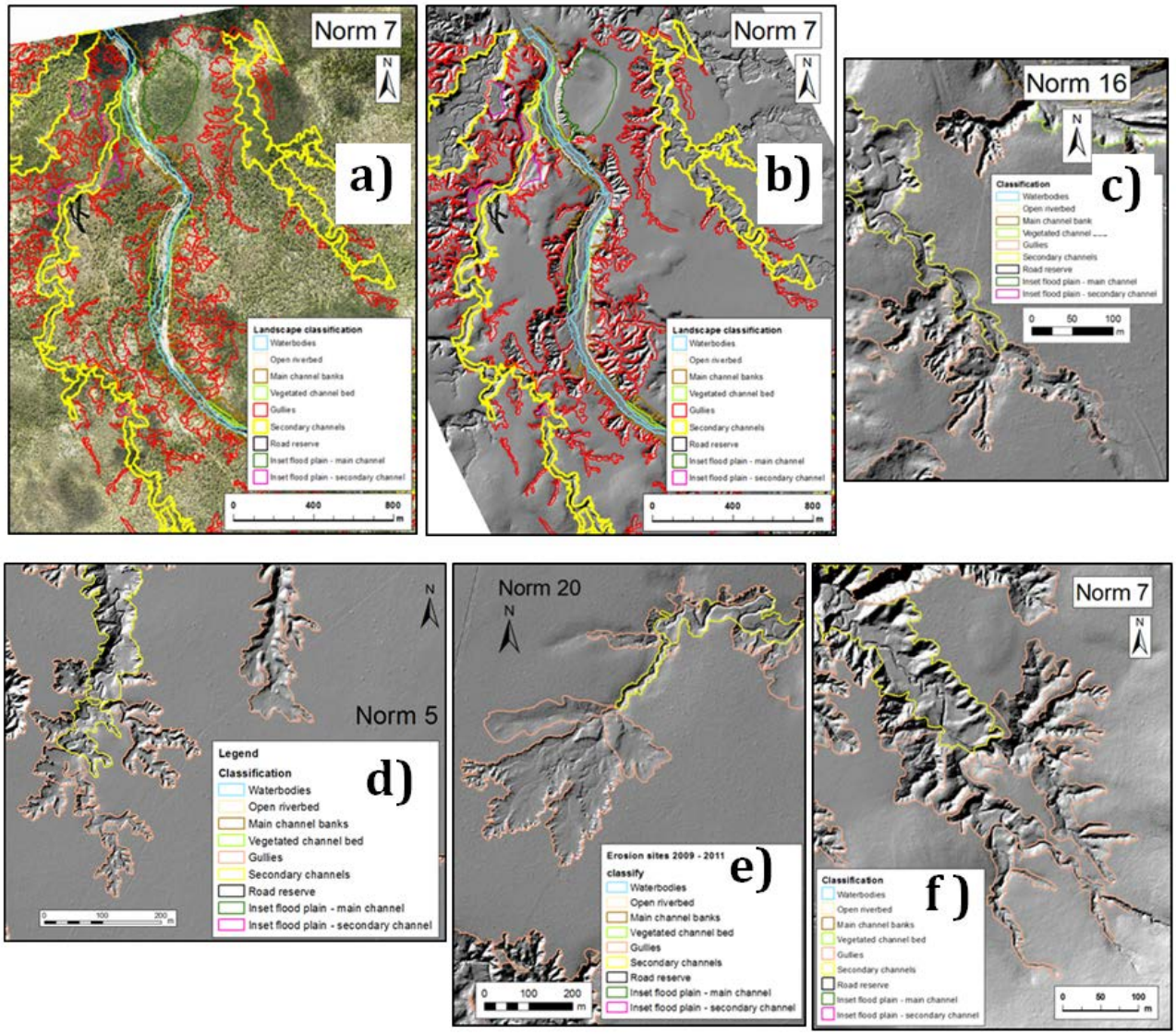

Figure 12: Location E (figure 7). Class 6 – Secondary Channels. These are transitional forms between gully and creek. Side wall retreat has significantly slowed and a self-forming alluvial channel has developed. Where to place the boundary between a secondary channel and a gully is partially subjective, but secondary channels are distinctive. They are linear to sinuous, ephemeral vegetated streams that function more as sediment transfer zones rather than sediment source zones function of gullies. They exist at a range of scales, from channels within localised gully complexes to channels with significant length and catchment area.

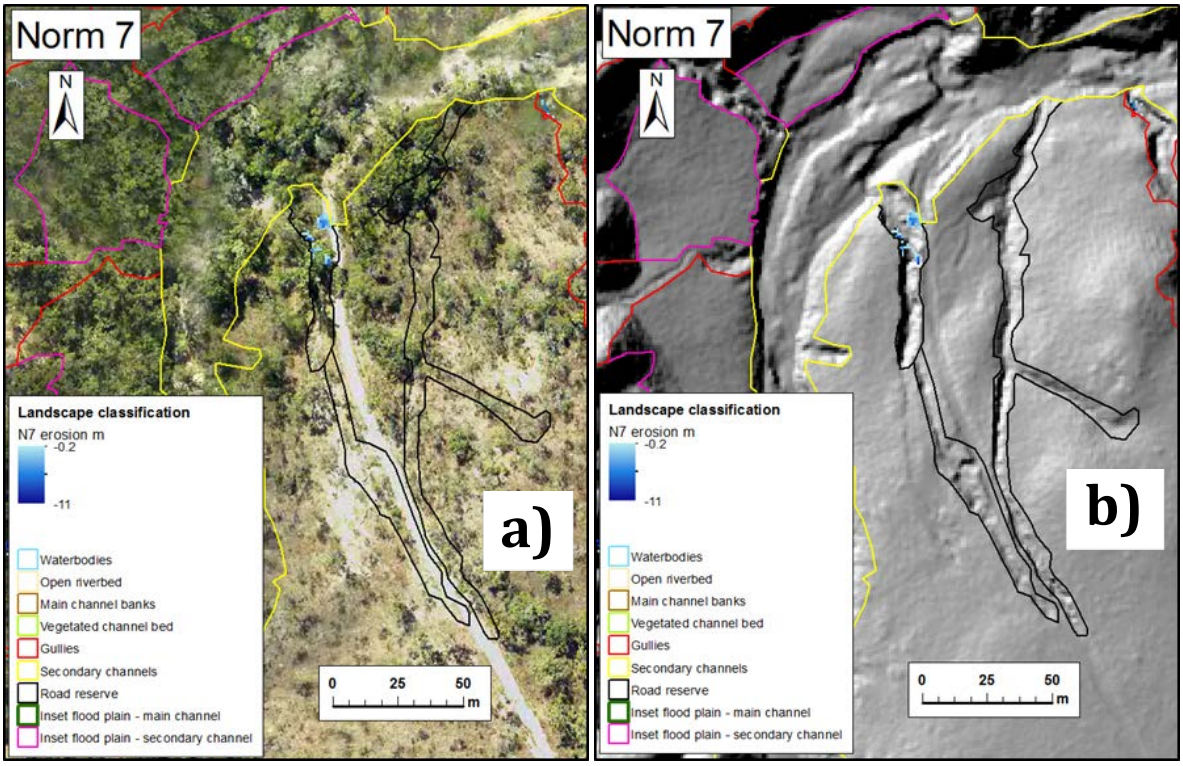

Figure 13: Location F (figure 7). Class 7 – Road Reserve. While erosion of road surfaces was below detectable limits from this LiDAR data, the effects of gullying from runoff from road drainage was measurable. Roads and tracks catch and channel water moving across otherwise un-eroded slopes, resulting in higher flows to the drainage outlet.

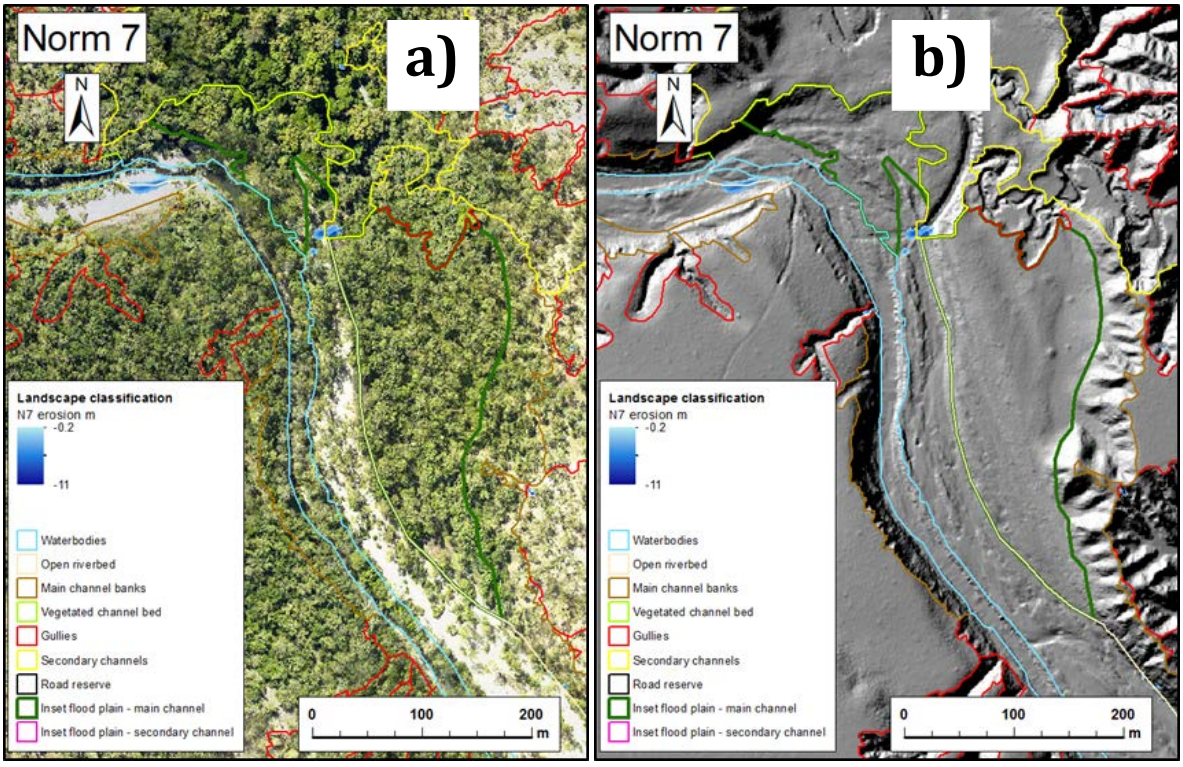

Figure 14: Location G (figure 7). Class 8 – Main Channel Inset Floodplain. Relatively large vegetated and mostly flat areas elevated above the main channel bed, but below the upper floodplain surface. These surfaces have minimal evidence of fluvial scour. Several levels of inset floodplain may exist

between current channel bottom and the upper floodplain surface. Elevations above main channel bed ranged from 2 to 12 metres.

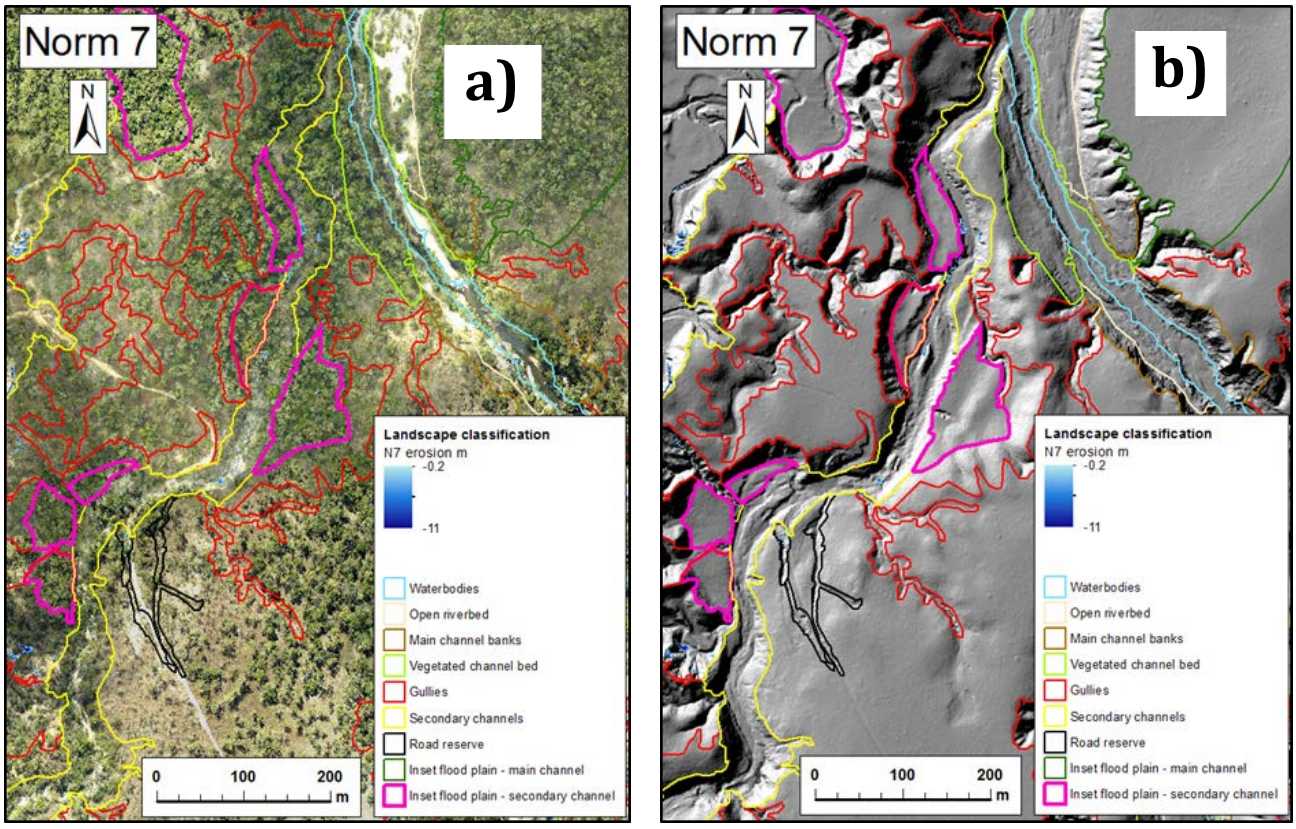

Figure 15: Location H (figure 7). Class 9 – Secondary Channel Inset Floodplain. Vegetated, mostly flat areas with minimal evidence of fluvial scour, adjacent to secondary channels, elevated above secondary channel beds, but below the level of surrounding alluvial floodplain surface into which these secondary channels are incised.

3.2 Erosion within Landscape Unit Classes

A change detection analysis between the 2009 and 2011 LiDAR (described below) was used to assess the volumetric change within all landscape units, other than water bodies (water bodies were excluded as the LiDAR in this instance cannot collect terrain data through water). The change detection dataset required manual editing. Each landscape class has a different geomorphic context and the editing was adjusted accordingly. Statistics for erosion, deposition, CHM ad PFC in each block were calculated for all the pixels within each landscape unit polygon.

Other components of this study involved particle size and bulk density analysis of different landscape units (see main report, appendix 9 and 15). The average proportion of fine sediment (<63um) from the material that makes up a landscape unit is shown in Table 6 and the bulk density is shown in Table 7. The bulk density values were used to convert the volumetric change to loads (tons) and the proportion of fine sediment was used to divide the loads into suspended sediment and bedload sediment.

Table 6: Proportion of fine sediment of different landscape units.

Landscape Unit	Average % <63µm	1 Standard Deviation
Bench	26.5	11.5
Gully Wall	61.9	19.7
Channel Bank	54.3	33.8
Secondary Channel Bank	33.7	10.4
Coastal Plain	80.3	31.8

Table 7: Bulk density of different landscape units.

Landscape Unit	Mean Bulk Density g/cm³	1 Standard Deviation
Bench	1.44	n/a
Crocodile Creek Secondary Channel	1.60	0.08
Gully Wall	1.94	0.23

The following figures (16, 17 and 18) summarise the proportional contribution of landscape units by volume of erosion measured within repeat LiDAR blocks. Note that LiDAR acquisition was targeted toward alluvial areas and therefore the results shown in these figures are biased toward alluvial areas and are not representative of the whole catchment and differ significantly.

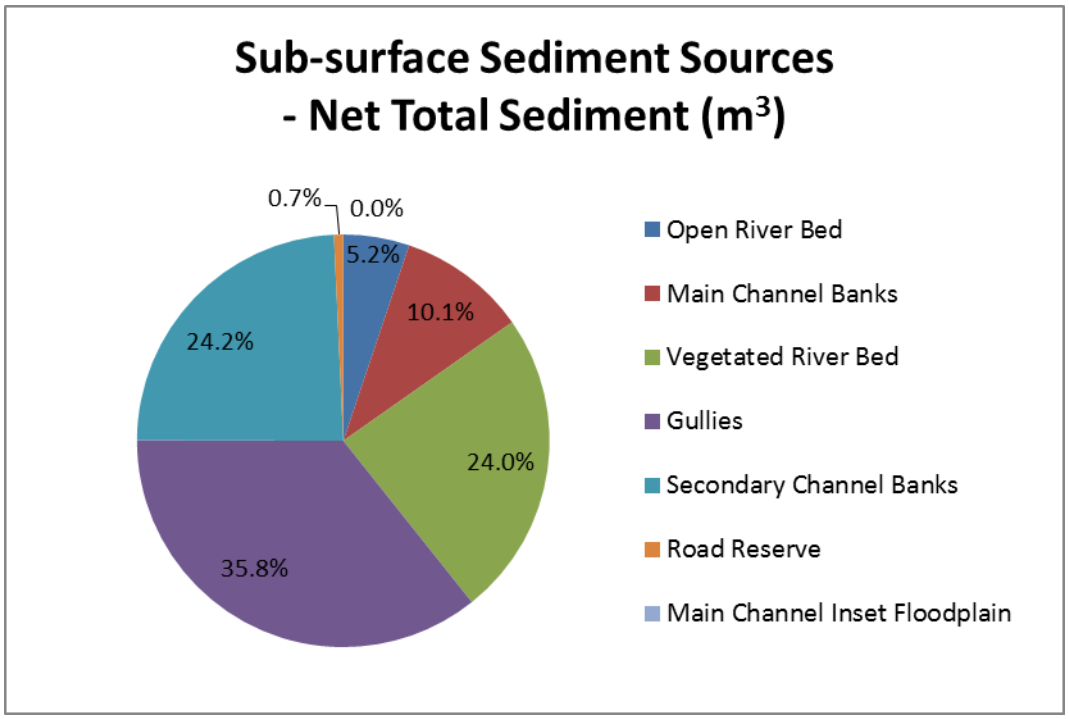

Figure 16: The relative proportions of erosion by volume of sub-surface sediment sources within landscape units summed for all repeat LiDAR blocks.

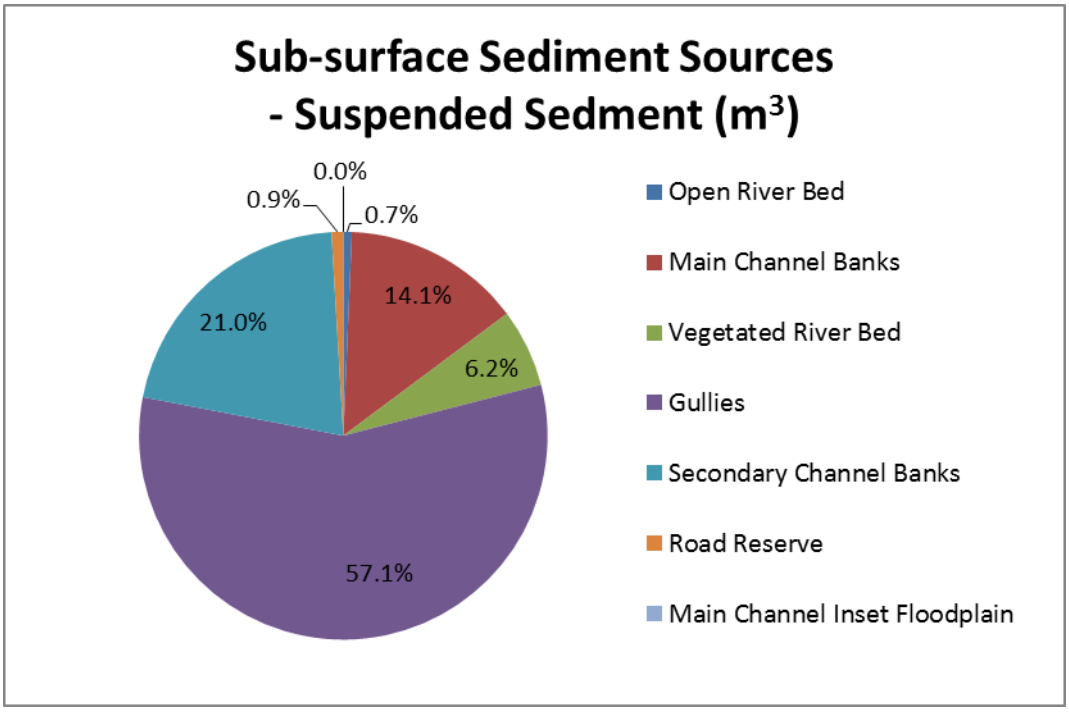

Figure 17: The relative proportions of erosion by volume of sub-surface fine sediment (suspended sediment) sources within landscape units summed for all repeat LiDAR blocks.

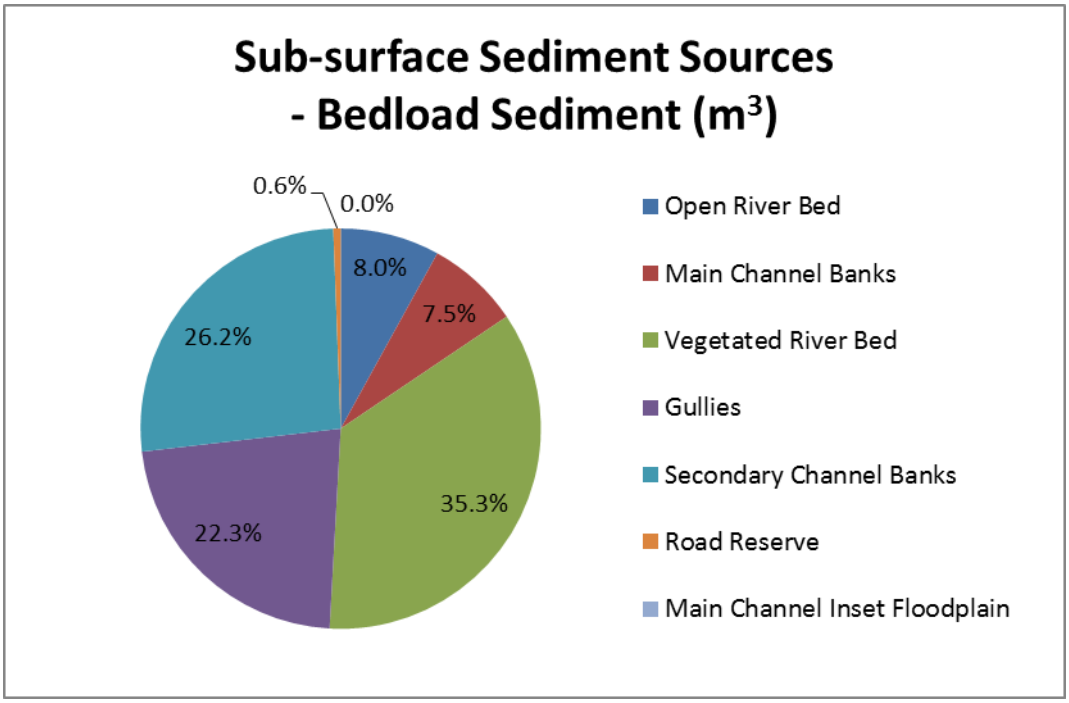

Figure 18: The relative proportions of erosion by volume of sub-surface coarse sediment (bedload sediment) sources within landscape units summed for all repeat LiDAR blocks.

4. Change Detection Analysis – Measurement of Short Term Sediment Production

A change detection analysis was undertaken to determine the volume of surface change that occurred between the 2009 and 2011 LiDAR acquisition dates. A change detection analysis involves subtracting one raster dataset from another and examining the difference. In this study the analysis involved the difference between the digital elevation models (DEM) derived from the 2009 and 2011 LiDAR data. The volume change is interpreted as erosion or deposition. The initial change detection analysis highlighted that the 2009 and 2011 LiDAR data contained substantial random error from measurement limitations and substantial systematic error from processing methods. These errors produced so many false positives in the change detection dataset that the signal to noise ratio becomes too low to separate actual change from error.

Data accuracy and processing issues included:

- There was a difference of spatial registration of up ~3m between the 2009 and 2011 data. That is, obvious locations visible in 2009 and 2011, such as a road or the edge of a gully, were misaligned up to ~3m. This type of error is observed in the DEM difference rasters as an unnatural pattern of erosion on one side of a gully and deposition on the other (see figure 22).
- The point cloud LiDAR data is a mass of points with X, Y, and Z values that represent anything the laser struck, be that vegetation, cattle, buildings, or the ground. Classifying points as ground or non-ground points is an involved process. It begins with an automated process which has sensitivity adjustments and settings done when generating the point cloud from the raw LiDAR data. The automated classification can be followed by manual reclassification. The points classified as ground are used to generate the DEM which represents the ground surface. Inconsistent classification creates errors in the change detection analysis, such as;
    - Areas of complex gully topography occasionally had areas of ground surface removed as vegetation. These areas were either at the edge of gullies (figure 19 and figure 20) or remnant pedestals within gullies (figure 21 and figure 22).
    - In consistent vegetation removal on heavily vegetated steep slopes within gullies creating DEM difference errors of up to 1m.
- Vertical misalignment between mosaicked swaths in the same block, resulting in step changes in values in the difference raster.

These data accuracy and processing issues are a consequence of operating in remote areas and cost-benefit decisions and are not inherent issues with the LiDAR acquisition or the equipment operation and were addressed in conjunction with the data supplier (RPS), including being contracted to reprocess some of the 2009 LiDAR to match the 2011 LiDAR processing, which required several iterations. Consequences of reprocessing the 2009 LiDAR data were that the landscape unit polygons (that were hand digitising on the original 2009 data) and the CHM and PFC rasters had to be shifted on a block by block basis to

align with the reprocessed 2009 data. Notably, a GPS base station located at Cooktown airport was the source of the LiDAR GPS differential correction data during the 2009 LiDAR acquisition. Most of the Normanby LiDAR blocks are beyond the recommended 30km radius (Saylam, 2009) from this base station. This is thought to be a significant source of the spatial positioning error observed between the 2009 and 2011 data.

DEM difference rasters (Table 8) were supplied for 14 blocks with a total area of 163.1 km^2, and an average 11.6 km^2 per block.

Table 8: Raster data for 2009 and 2011 from LiDAR surveys in the Normanby catchment.

Product	2009 Data	2011 Data
Orthophoto	Cell size 0.125x0.125m, RBG	
Digital Elevation Model (DEM)	Cell size 1x1m, TIFF, floating point	Cell size 1x1m, TIFF, floating point
Hillshade Raster (HS)	Cell size 1x1m, TIFF, floating point	Cell size 1x1m, TIFF, floating point
Canopy Height Model (CHM)	Cell size 1x1m, TIFF, floating point	
Projected Foliage Cover (PFC)	Cell size 1x1m, TIFF, floating point	
Difference 2009-2011		Cell size 1x1m, TIFF, floating point

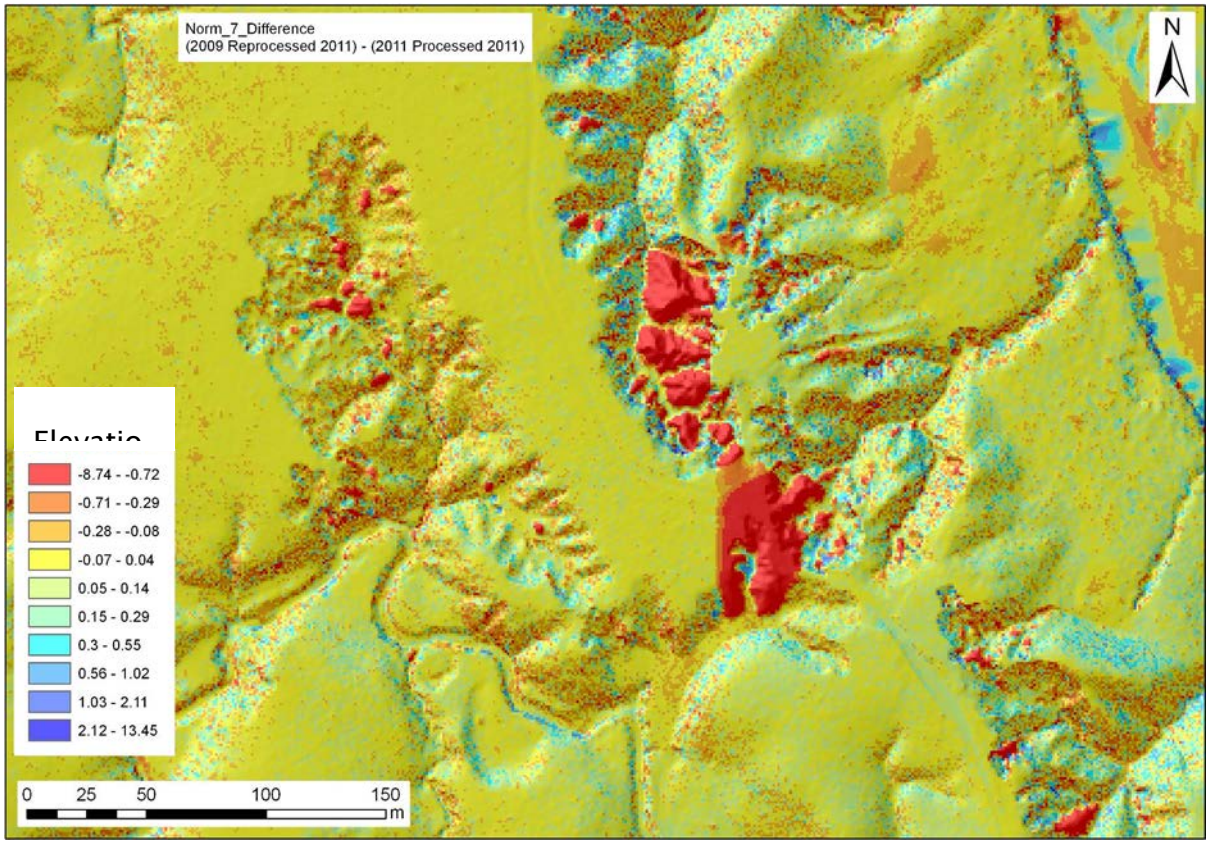

Figure 19: Example of error in the initial change detection difference data. This example is a result of incorrect classification of LiDAR ground points as non-ground points in the 2009 LiDAR data. The large negative values of elevation difference are false and were not present in the difference data after the 2009 LiDAR was reprocessed to the 2011LiDAR specifications. Figure 20 shows this area as a hillshape relief image.

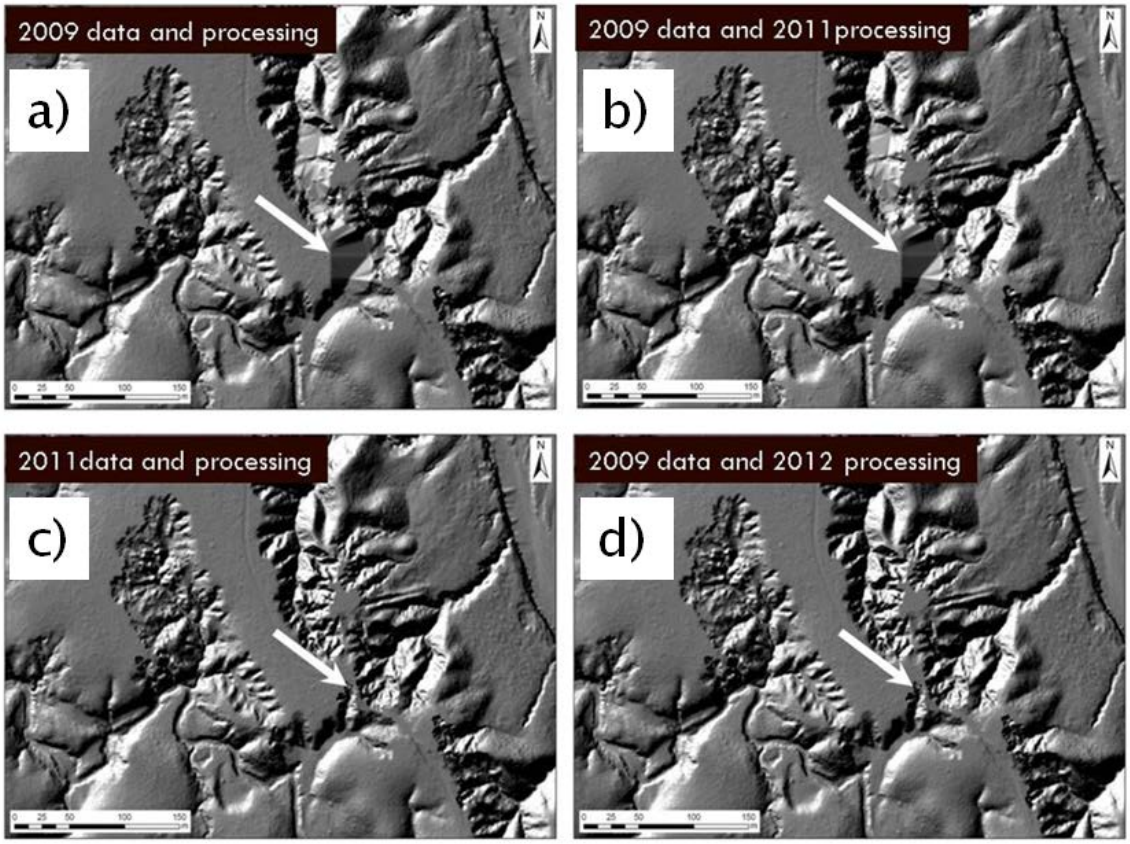

Figure 20: The cause and solution of the error shown in figure 19 is evident in these images. The 2009 data had areas of incorrect ground surface representation, arrow in a). Therefore when subtracted from the 2011 surface in c) these areas produce a significant elevation difference that was only an artifact of the inconsistent LiDAR processing methods. The first reprocessing iteration b) did not resolve the error, the final iteration d) remove these artifacts from the DEM data.

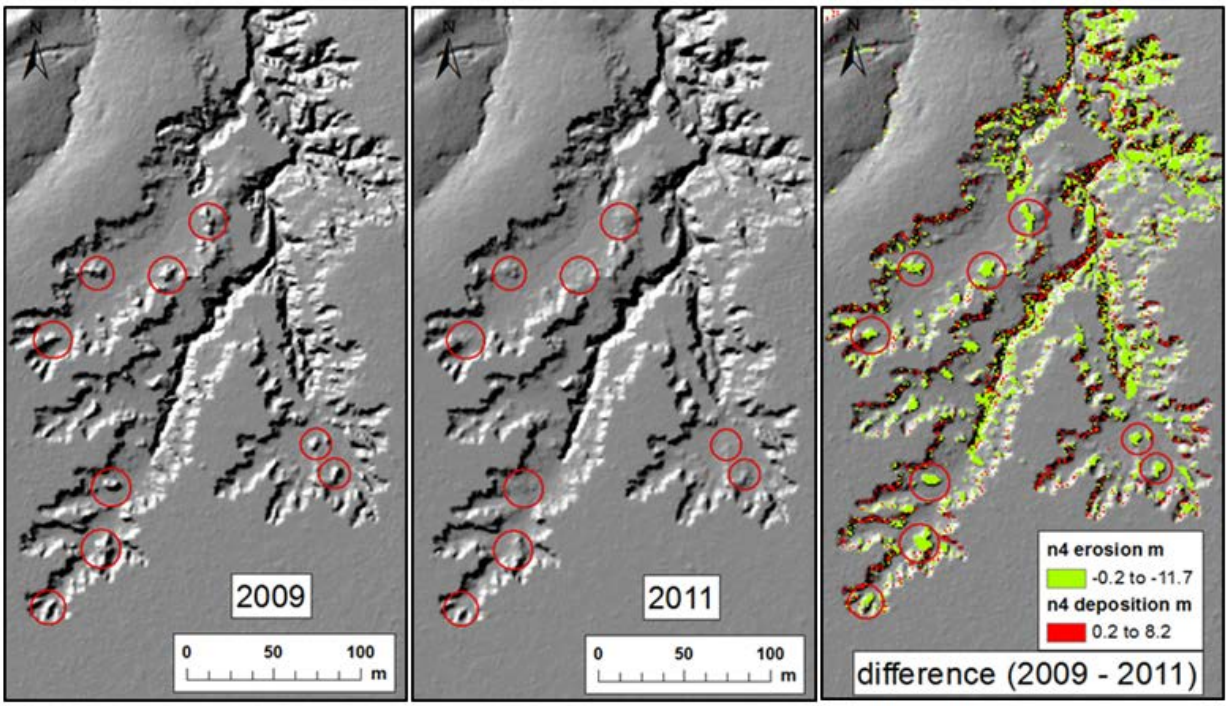

Figure 21: Gullies often have pedestals and peninsular which are remnants of the original land surface. They can be tall isolated features and, not surprisingly, were occasionally classed as

structures or vegetation in the LiDAR point cloud by the automated classification processes. Several of these features were visited on the ground (figure 22) to verify that they had not eroded in 2011 and that the DEM data contained artifacts of the LiDAR processing methods. This misrepresented of the ground surface produced error in the change detection data.

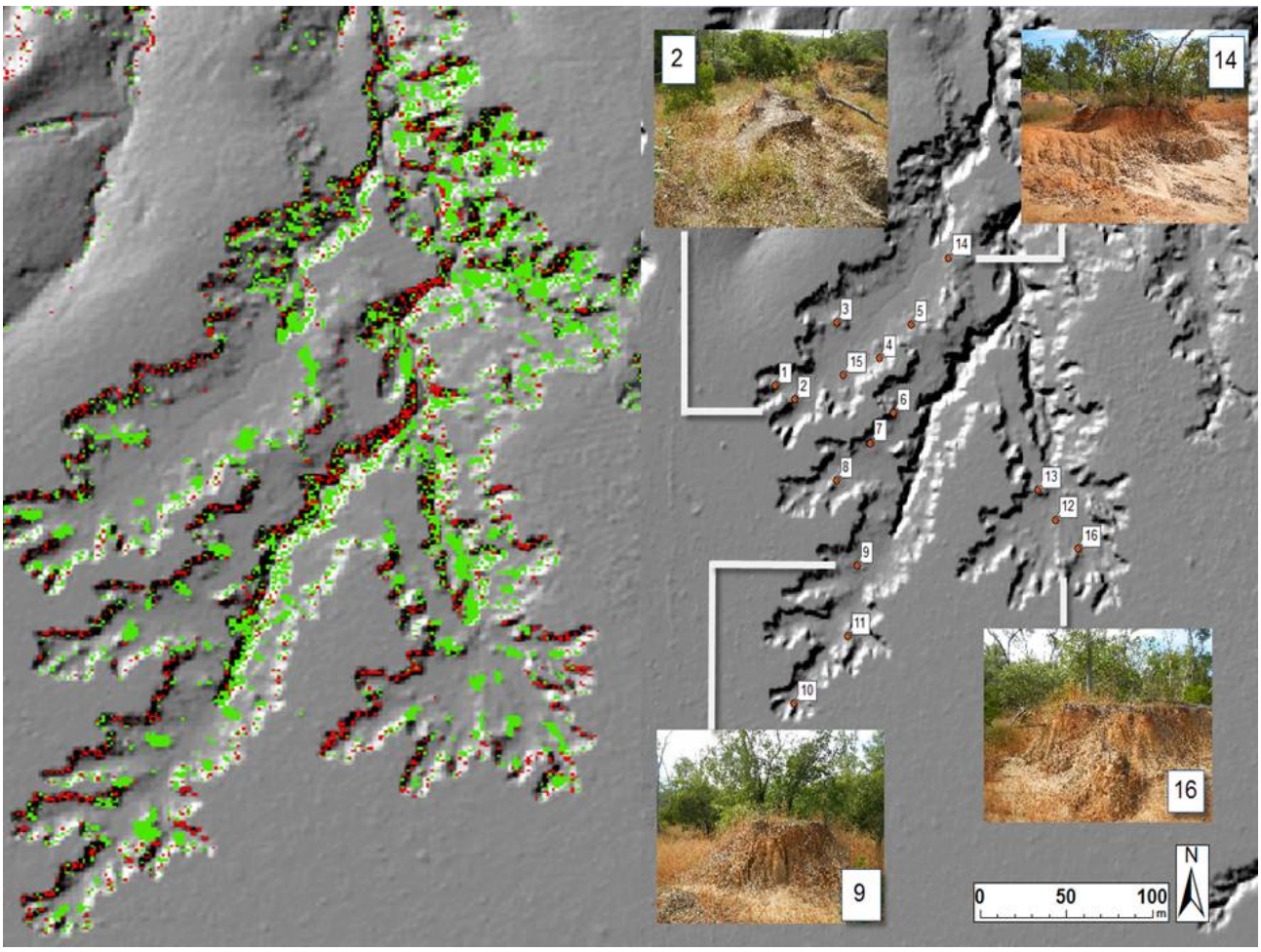

Figure 22: Several remenant pedestal features (figure 21) that were present in the 2009 DEMs, but not in the 2011 DEMs, i.e. appeared to have been eroded, were visited on the ground to verify the DEM data. As can be seen in the photo, these features were demonstrably still present. Their presence informed the design of the LiDAR reprocessing methods and the reprocessed data had more realistic representations of the remnant pedestal features. The green in the image represents elevation decrease and the red represents elevation increase between 2009 and 2011. Note the unnatural grouping of red on some faces of the gully and green on others. This is an artefact of spatial mis-registration of the LiDAR data mentioned above. (Photos: Jeff Shellberg).

4.1 Reduction of Background Noise in Change Detection Data

A two stage process was used to remove noise, or random error, from DEM difference rasters.

Firstly, to determine if difference raster data had systematic elevation offset the rasters were sampled in twenty 100 X 100m polygons which were located on floodplain surfaces where it was considered that close to no erosion had occurred between 2009 and 2011.

The average difference of the sample was added or subtracted to an entire difference raster to correct for any offset (figure 23).

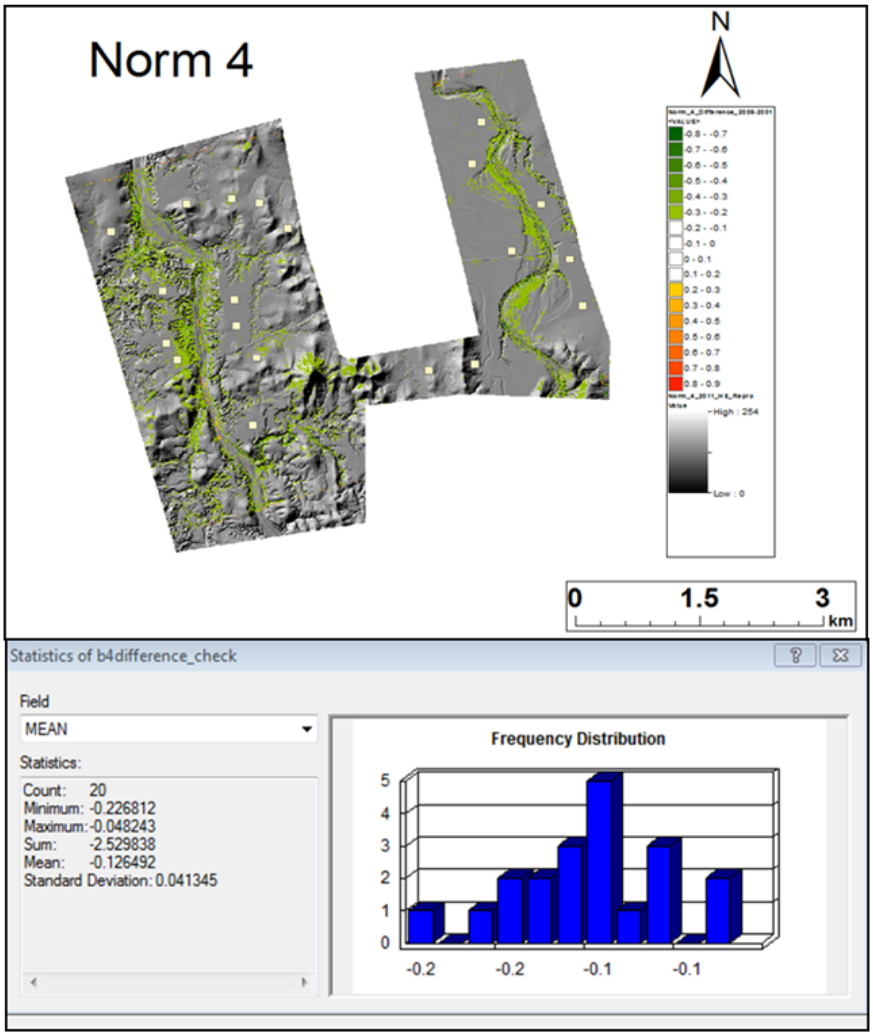

Figure 23: Example of the procedure used to correct for vertical offsets in difference rasters. Elevation statistics were derived for a sample of twenty 100 X 100m squares located on floodplain surfaces that were considered not to have changed between the 2009 and 2001LiDAR acquisition. The difference raster was adjusted uniformly by mean offset of the sample.

Secondly, all values in the range 0.2m to -0.2m were eliminated from the difference rasters as this is within the vertical error range of LiDAR data. The national standard for LiDAR vertical accuracy is now ≤ ± 30cm at the 95% confidence interval, previously ≤ ± 15cm at the 68% confidence interval (GA, 2010). Therefore, any erosion that did occurred in the LiDAR blocks within this 40 cm range was the beyond the detection limit of this study. This excludes small amounts of erosion that occurred on gully faces, but also, types of erosion that only occur by small degrees. Surface scalding on bare earth, minor scouring of floodplains, deposition of mud drapes, or most types of hillslope erosion were beyond detection. These are important erosional processes and in future studies data quantifying them will be an important additional layer of understanding to sediment sources and sinks. As would be expected there was no elevation change (i.e. erosion/deposition) on floodplain surfaces after the removal of the 0.2m to -0.2m range.

4.2 Aggressive Filtering and Editing of Change Detection Data

Larger surface changes between 2009 and 2011 mostly associated with gully and bank erosion are within the detectable range of the methods used here. The DEMs derived from the LiDAR data have a 1x1m cell size and changes involving a square metre or more are, for the most part, detectable. Many gullies in the study area have rapid head scarps retreat rates, greater than 1m per year, and are generally more than 1m deep. Similarly channel banks tend to be greater than 1m deep and hence channel migration greater than 1m in the two year interval between LiDAR surveys is detected within the resolution of the data.

While the filtering of the difference raster in the range of ± 20cm significantly reduced the background noise on the floodplain surface, within the gullies themselves the signal to noise ratio was particularly low. Many of the gullies are heavily vegetated and with the degree of background noise it would appear that LiDAR penetration through the vegetation and the classification of ground points was not sufficiently consistent within vegetated gullies between the 2009 and 2011 LiDAR acquisition and processing.

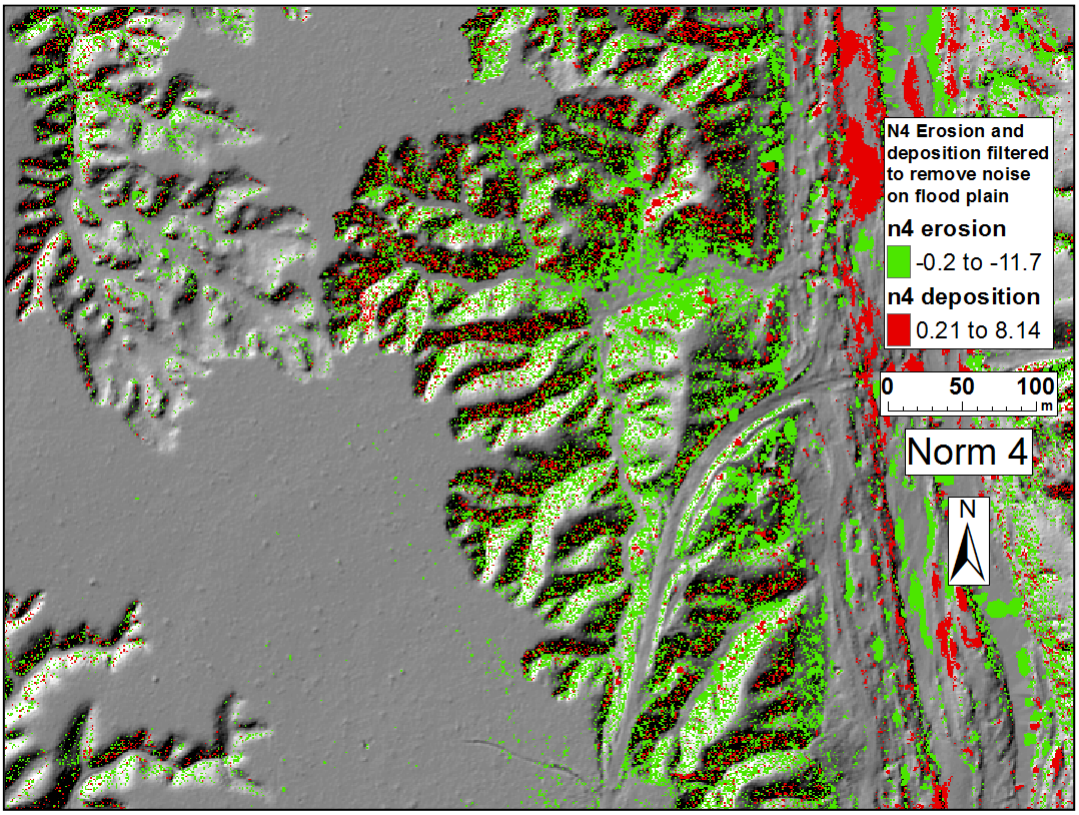

Figure 24: Example of the degree of background noise in the difference raster within the vegetated gullies. Note that the upper extents of the gully to the top left of the image shows much less evidence of noise. This is an area of gully containing little or no vegetation.

To address the background noise more filtering steps were undertaken. Elevation changes greater than 1m were assumed to be actual elevation change. Any pixels with less than 1m of change were excluded from the difference raster. It was assumed that any isolated pixel, even with a change greater than 1m did not represent actual change, but possibly a LiDAR artifact such as a laser return from a tree trunk or termite mound in one LiDAR acquisition and not the other. All isolated cells were excluded from the difference raster. Remaining

pixels had a 3 metre buffer applied and any pixels with elevation change within this buffer that had been excluded in the previous two steps where reintroduced to the difference raster (figure 25). This was to include pixels on the cusp of advancing gully headwalls with a headwall height greater than a metre. This filtering procedure was done for positive elevation change and negative elevation change, producing a deposition raster dataset and an erosion raster dataset.

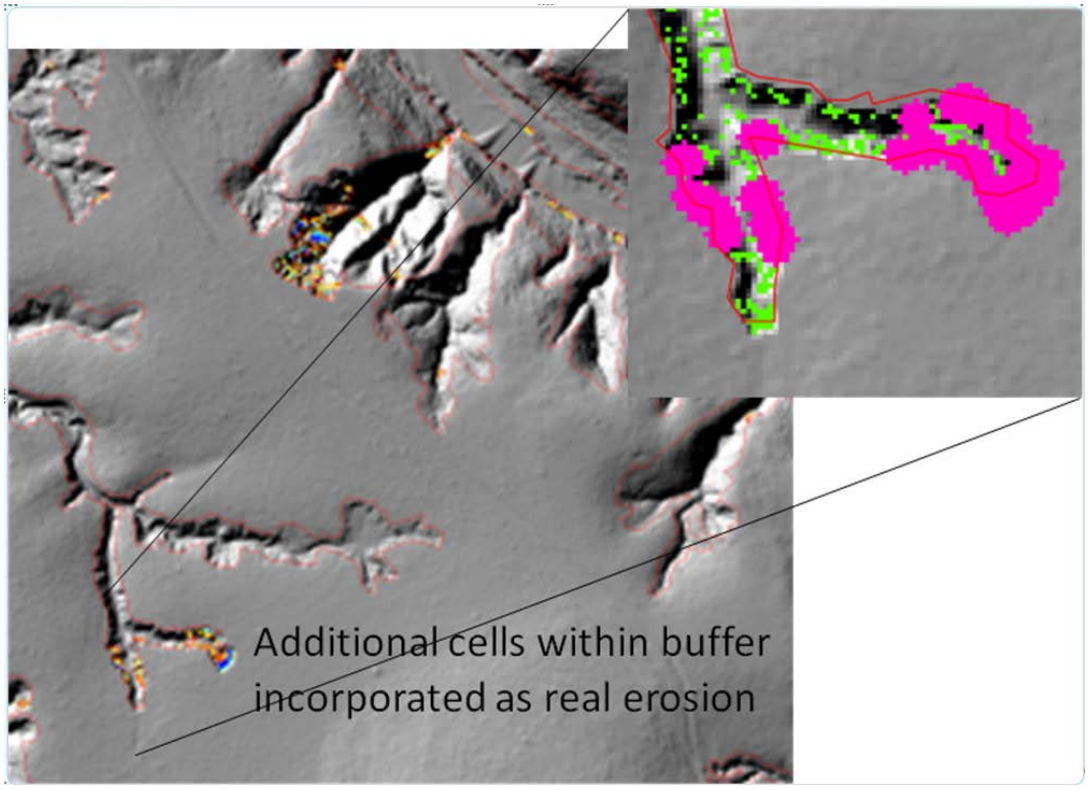

Figure 25: Example of the process for filtering elevation change background noise at a gully headwall. The green cells at the gully headwall that did not meet the initial criteria for inclusion difference raster dataset were subsequently reincorporated in the manual editing phase.

All patches of erosion and deposition pixels were converted to polygons and manually assessed to determine whether they were likely to be actual erosion/deposition or otherwise. The criteria for accepting a polygon as erosion was; a) that it should sit on an obvious flow path or be connected to a flow path at higher flows, b) be a solid patch without small random inclusions of non-erosion pixels, c) be at a gully head wall, or d) considered to be where erosion is likely to occur on a bank, bench, mid channel island, etc. Polygons that did not meet these criteria were excluded.

It was assumed that if deposition was detected that it must exclusively be the deposition of bedload material as deposition of fine material, such as mud drapes, is below the detection limit of the LiDAR data and filtering methods use here. The criteria for accepting a deposition polygon was that it must logically occur at a location where it would be feasible for bed-material load to accumulate within the two year interval. So in addition to being located within a channel or associated with a channel, the polygon needed to be a discrete solid patch, without small random inclusions of non-deposition pixels.

As an example, in Normanby Block 4 these hand editing processes reduced the area of erosion from 16.8 ha to 5.9 ha and area of deposition from 34.6 ha to 3.9 ha.

The final rasters of erosion and deposition were produced by extracting the height adjusted difference raster data within the hand edited erosion and deposition polygons.

A consequence of the extensive filtering and editing described above to produce erosion and deposition data that has a reasonable level of confidence is that only major erosion (gully headwall retreat, incision, channel expansion, lateral channel migration, mass movement, etc.) and major bedload deposition are represented. Therefore the erosion and deposition data layers are considered to be highly conservative in quantifying surface changes between 2009 and 2011.

4.3 Ground Validation at Selected Gullies

A series of gullies that changed significantly in the erosion dataset between the 2009 and 2011 were inspected on-ground to validate that this change was actually erosion. Figures 26 – 29 have hillshade relief images and ground photos. Overlain on the hillshade image is the final erosion raster dataset (small red sections at head of gullies). These examples demonstrate that the filtering and editing procedure is capturing major gully erosion between 2009 and 2011. Ground inspection also highlights the substantial amount of subtle change associated with scalding and gully wall processes which is not being captured in the LiDAR data and the change detection analysis.

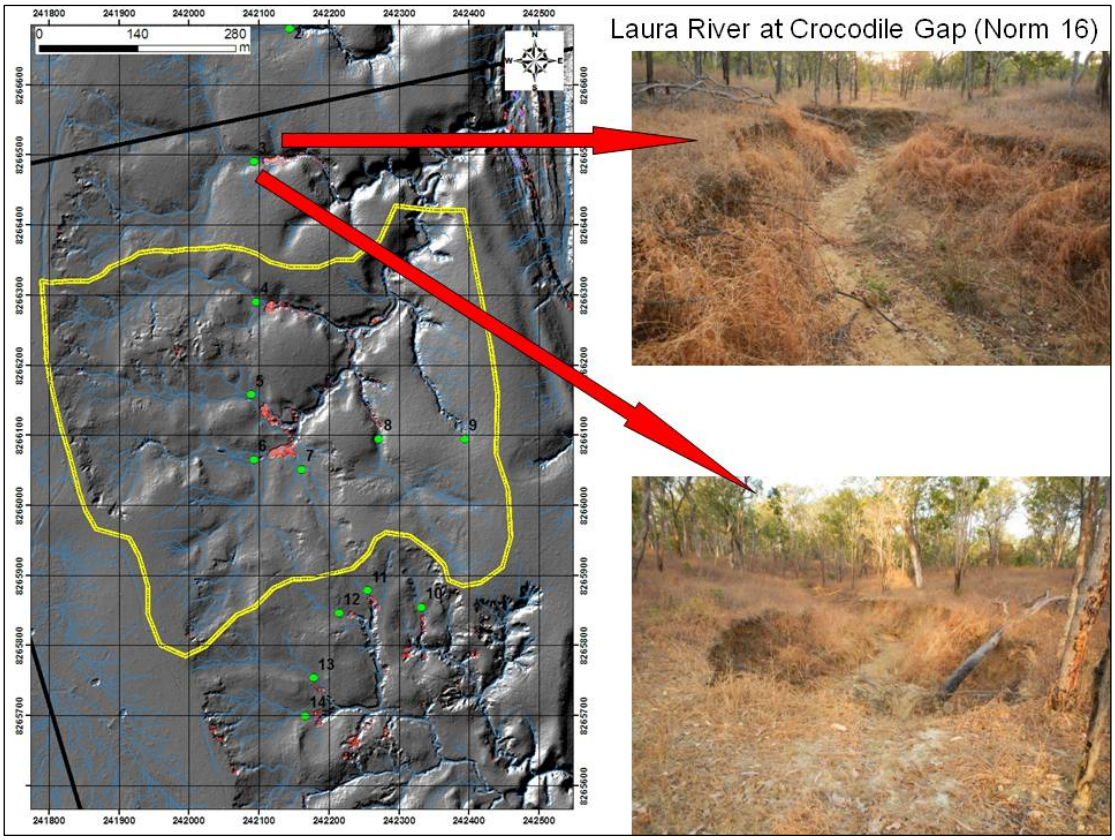

Figure 26

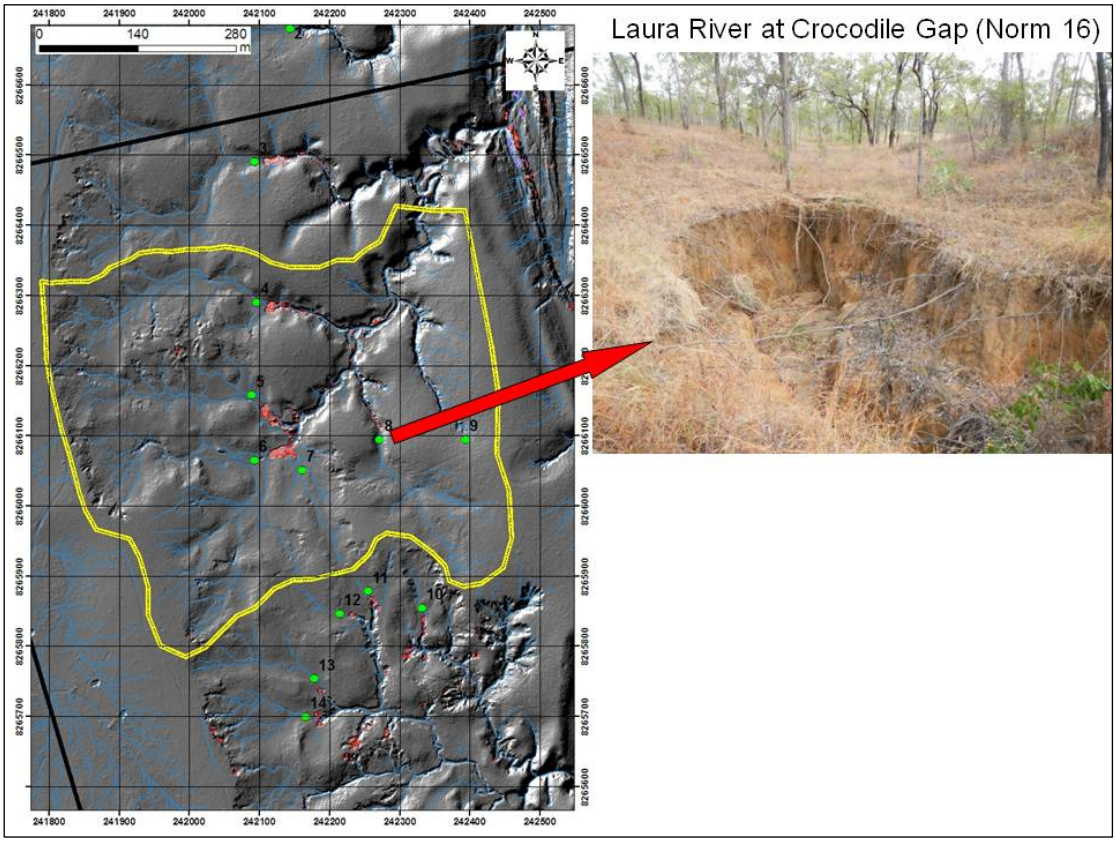

Figure 27

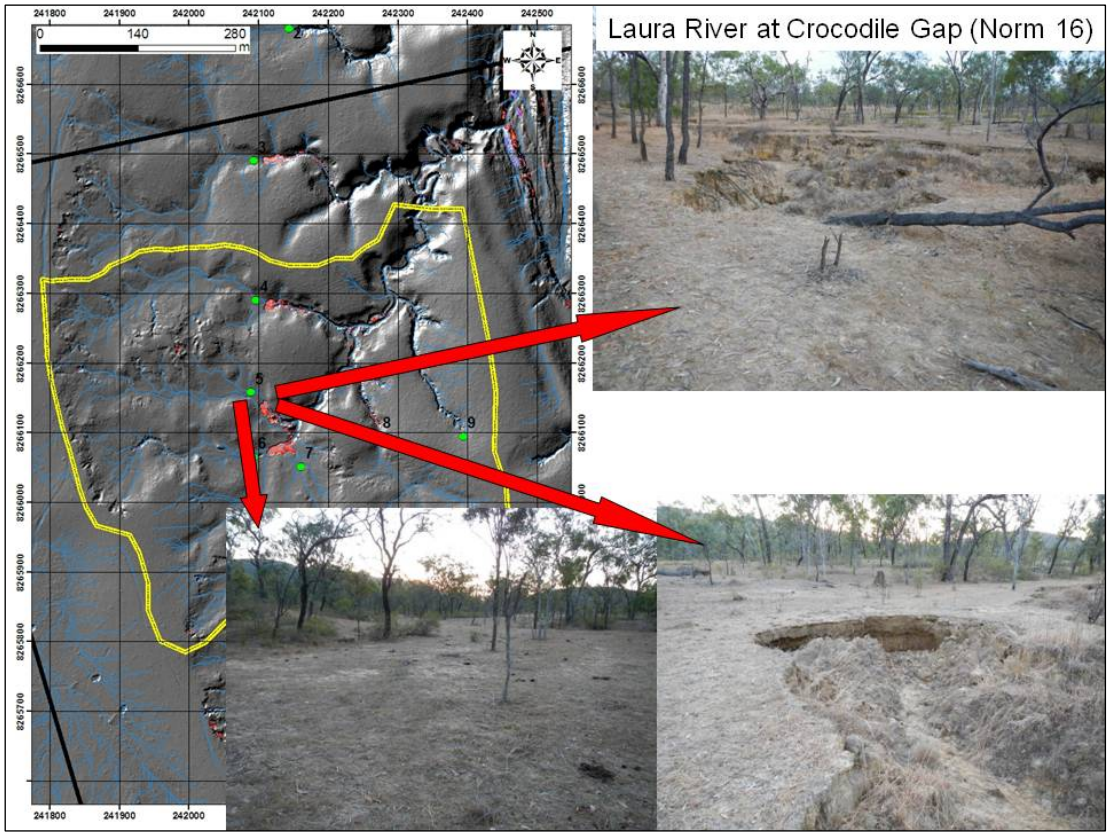

Figure 28

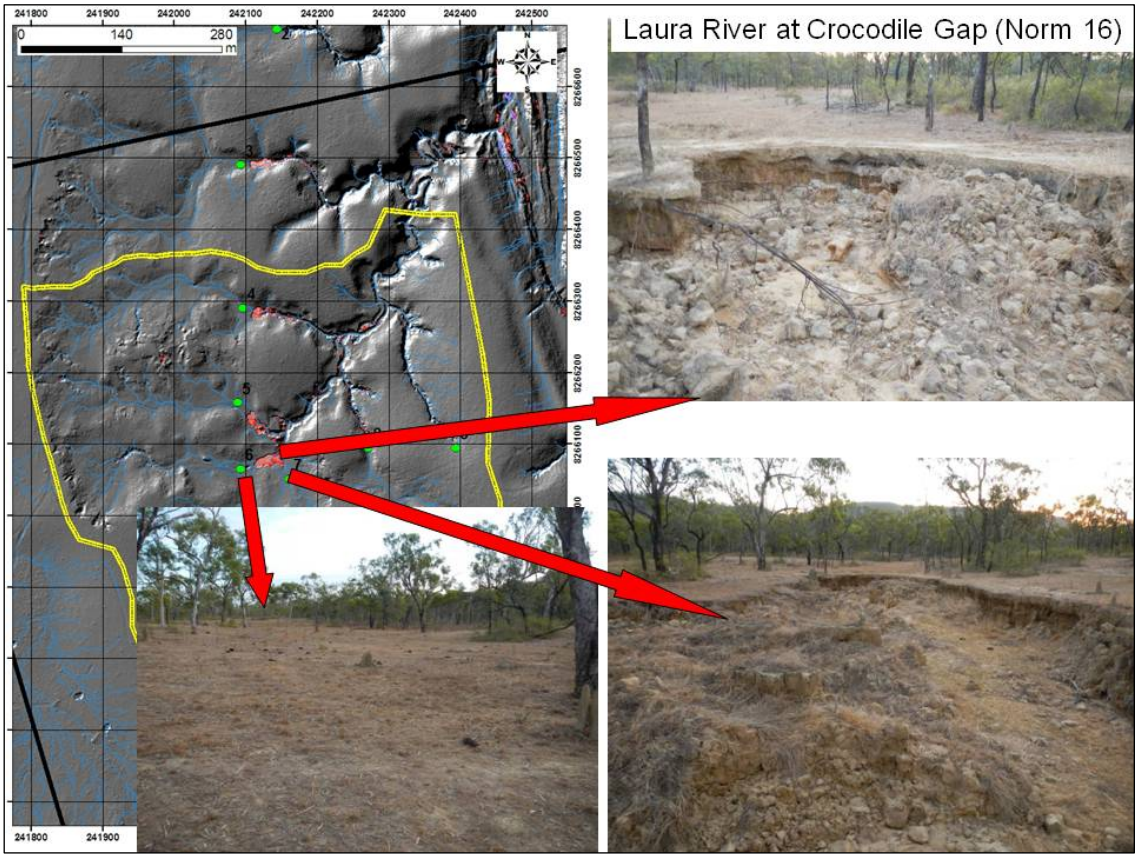

Figure 26 – 29: Hillshade relief images and ground photos at gully site visited to validate LiDAR derived change detection analysis. Overlain on the hillshade image is the erosion raster dataset (small red sections at head of gullies). These gullies were identified as changing significantly in the LiDAR data between 2009 and 2011. (Photos: Jeff Shellberg).

References

Please also see main document, or visit the website: **http://www.capeyorkwaterquality.info**

Brierley, G.J., Fryirs, K.A., 2005. Geomorphology and river management: application if the river styles framework. Blackwell Publishing, Victoria, Australia.

Brooks, A., Spencer, J., Knight, J., 2007. Alluvial gully erosion in Australia's tropical rivers: a conceptual model as a basis for a remote sensing mapping procedure. In: A.L. Wilson, R.L. Dehaan, R.J. Watts, K.J. Page, K.H. Bowmer, A. Curtis (Eds.), Proceedings of the 5th Australian Stream Management Conference, pp. 43-48.

Brooks, A.P., Spencer, J., Shellberg, J.G., Knight, J., Lymburner, L., 2008. Using remote sensing to quantify sediment budget components in a large tropical river - Mitchell River, Gulf of Carpentaria, Sediment Dynamics in Changing Environments (Proceedings of a symposium held in Christchurch, New Zealand, December 2008). IAHS Publication, pp. 225-236.

GA, G.A., 2010. ICSM LiDAR Acquisition Specifications and Tender Template. Intergovernmental Committee on Surveying and Mapping.

Saylam, K., 2009. QUALITY ASSURANCE OF LIDAR SYSTEMS – MISSION PLANNING, ASPRS 2009 Annual Conference. American Society for Photogrammetry and Remote Sensing, Baltimore, Maryland.